MANUFACTURE OF COMPLEX GEOMETRY COMPONENT FOR ADVANCED MATERIAL STIFFNESS

A Thesis

presented to

the Faculty of California Polytechnic State University,

San Luis Obispo

In Partial Fulfillment

of the Requirements for the Degree

Master of Science in Mechanical Engineering

by

David Russell Bydalek

March 2018

COMMITTEE MEMBERSHIP

TITLE:	Manufacture of Complex Geometry Component for Advanced Material Stiffness
AUTHOR:	David Russell Bydalek
DATE SUBMITTED:	March 2018
COMMITTEE CHAIR:	Joseph Mello, Ph.D. Professor of Mechanical Engineering
COMMITTEE MEMBER:	Eltahry Elghandour, Ph.D. Associate Professor of Mechanical Engineering
COMMITTEE MEMBER:	Declan Hayes Director of Engineering

ABSTRACT

Manufacture of Complex Geometry Component for Advanced Material Stiffness

David Russell Bydalek

The manufacture, laminate design, and modeling of a part with complex geometry are explored. The ultimate goal of the research is to produce a model that accurately predicts part stiffness. This is validated with experimental results of composite parts, which refine material properties for use in a final prototype part model. The secondary goal of this project is to explore manufacturing methods for improved manufacturability of the complex part. The manufacturing portion of the thesis and feedback into material model has incorporated a senior project team to perform research on manufacturing and create composite part to be used for experimental testing. The senior project was designed, led, and managed by the author with support from the committee chair.

Finite element modeling was refined using data from coupon 3-point bend testing to improve estimates on material properties. These properties were fed into a prototype part model which predicted deflection of composite parts with different layups and materials. The results of the model were compared to experimental results from prototype part testing and 3rd party analysis. The results showed that an accurate mid-plane shell element model could be used to accurately predict deflection for 2 of 3 experimental parts. There are recommendations in the thesis to further validate the models and experimental testing.

Keywords: Carbon Fiber Epoxy, Composite, FEA, Abaqus®, Classic Laminate Plate Theory, Shell Elements, Liquid Compression Molding, Resin Transfer Molding

ACKNOWLEDGMENTS

I would like to thank Dr. Mello for his support, guidance, and leadership to push the team to continue learning and progressing. Without his continued support this thesis would not have been possible. He truly embraces Cal Poly's "learn by doing" philosophy. I would also like to thank my other committee members, Dr. Elghandour for his guidance and recommendations to further this project, and Declan Hayes for providing funding for the project.

A special thank you to the student team, Nick Carlucci, Alex King, Caitlyn Pellemeier, and Eric Rodan. Their research is summarized in Chapter 1.2 and Chapter 5 of this thesis and was completed in 2017 and Q1 2018. Without their support and dedication, the manufacturing portion of this thesis would not have been complete.

Lastly, I would like to thank my wife who's love and support drove me to complete this thesis. She helped me to stay focused and supported all the hours of research required for a thesis. I am truly blessed to have her and it is together that we are jointly successful for endeavors such as these.

TABLE OF CONTENTS

Page

LIST OF TABLES

Page

LIST OF FIGURES

Page

1 INTRODUCTION

Our Customer has been working to improve stiffness of a complex part, so that deflection can be minimized. Traditionally, this part is made of homogenous material, however a new application resulted in the need to explore alternate materials to meet the design requirements. Ultimately, the Customer's engineering team had decided the best way to solve this problem was to design the part out of carbon fiber epoxy. This would allow the team to take advantage of directional properties of the material in order minimize deflection from part loading.

The Customer had made prototypes of the part, but was unable to get the part modeling to match the actual manufactured part deflection. In many cases the predicted deflection was much less than the actual part. Additionally, the manufactured parts did not meet the design requirements for deflection. This is believed to be due to complex geometry and manufacturing of the part. Furthermore, the Customer does not have experience designing composite parts. The goal for the Customer is to create accurate numerical models to improve design, while finding a repeatable, and cost-effective manufacturing method.

Cal Poly Mechanical Engineering Department was contacted with a request to create a project to improve part modeling and manufacturing. The result is this Master's Thesis, which encompasses, modeling improvements, as well as the management, and organization of a Baccalaureate Senior Project. The Senior Project team's focus was on finding optimal manufacturing methods, and creating sample parts for improvement in numerical modeling.

The key design parameters for both projects are as follows:

1: Part envelope of approximately 340mm x 62.5mm x 2.56mm
2: Maximum part deflection under loading must be less than 450 µm
3: Part parallelism must be < 0.20 across an approximate length of 340 mm
4: Part may be no thicker than 2.56 mm
5: Operating temperatures up to 60 degrees Celsius
6: Manufacturing of the part must be scalable to ~200/qtr

Figure 1 shows a breakdown of the overall work flow and ownership of the project. The author had not taken an engineering composites or finite element course, so all theory was self-taught as part of the scope of work.

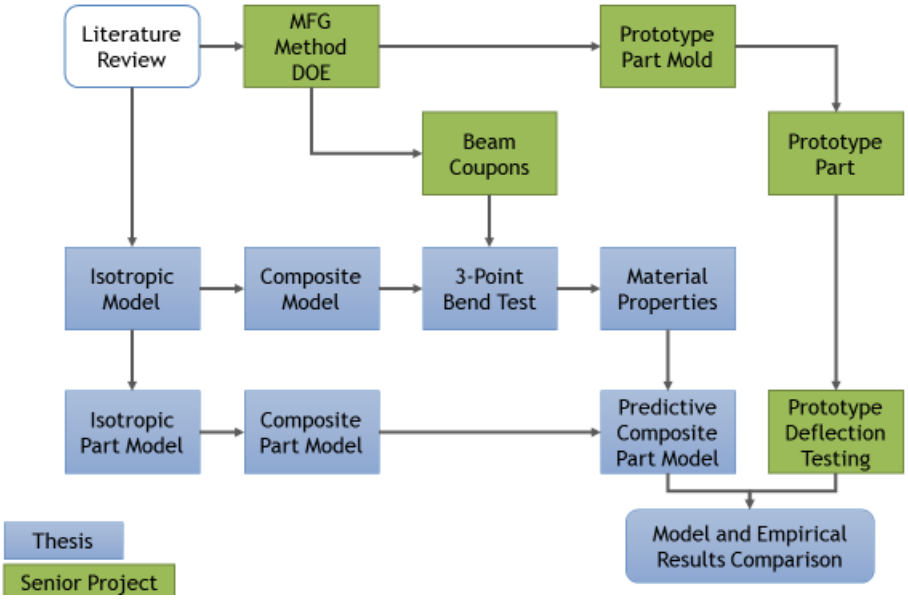

Figure 1 - Process flow for research and experimentation

2 LITERATURE REVIEW

2.1 Carbon Fiber Manufacturing

Carbon Fiber is a term that most people have heard of and tend to use freely to describe many lightweight materials with a weave appearance. The actual manufacture of carbon fiber is created from a polyacrylonitrile (PAN), rayon, or petroleum pitch. Approximately 90% of all carbon fiber is made from the PAN process, which will be described below ("How Is Carbon Fiber Made?"). The PAN process starts with the precursor PAN fiber and goes through a series of steps to re-align carbon atoms and remove unnecessary atoms. This process gives the carbon fiber strands their strength.

The manufacturing of the PAN precursor fiber is a complex process that is typically core IP of the carbon fiber manufacturers (Park and Heo). The general processing is similar to the textile industry. The study of the precursor manufacturing is beyond the scope of this research.

When a PAN precursor is ready to be processed, and turned into a carbon fiber, the first step is to thermally stabilize the material through a furnace. As shown in the process flow below, this is done at temperatures from 200-300 degrees Celsius. This helps the material to rearrange the atomic bonding through the introduction of oxygen molecules. The stabilization process helps to prepare the material for further heat treatment without melting the fiber material. The way in which the material is heated and stabilized varies from manufacturer to manufacturer (Park and Heo; "How Is Carbon Fiber Made?").

Now that the fibers are thermally stabilized, they go through a carbonizing process at temperatures of 1000 to 3000 degrees Celsius. The fiber is introduced into an oven that is in an inert environment, typically nitrogen or argon. The gas is then pressurized higher than atmospheric pressure. The result is the material expelling molecules in gaseous form such as water vapor, carbon dioxide, carbon monoxide, nitrogen, and hydrogen ("How Is Carbon Fiber Made?"). The temperature range varies based on the application of the carbon fiber being processed. Depending on the desired material characteristics, the fiber may go through a second heat treatment, called

graphitization. This process is used to create higher modulus carbon fibers (Park and Heo). The product of the carbonization and graphitization process is material with a crystalline carbon structure aligned along the length of the fiber.

The next step is to oxidize and clean the surface so that the fibers can better bond to epoxies used in the manufacture of composites. The oxidation process etches the surface and roughens the fiber to enable better bonding properties. There are many ways to oxidize the material, the method depends on manufacturer. Some examples include acid etching, electrolytic processing, or immersing in gases ("How Is Carbon Fiber Made?").

Lastly, the material is sized. This process coats the materials for protection and handling. The coated materials are then wound on bobbins, and processed through a spinning machine. This process is similar to many textile processes. The spinning process twists the fibers into carbon fiber yarn of specified size. After this, the yarn is then processed to make weaves of various types that can be purchased for production of composite parts ("How Is Carbon Fiber Made?") Figure 2 below, is visual example of the manufacturing process.

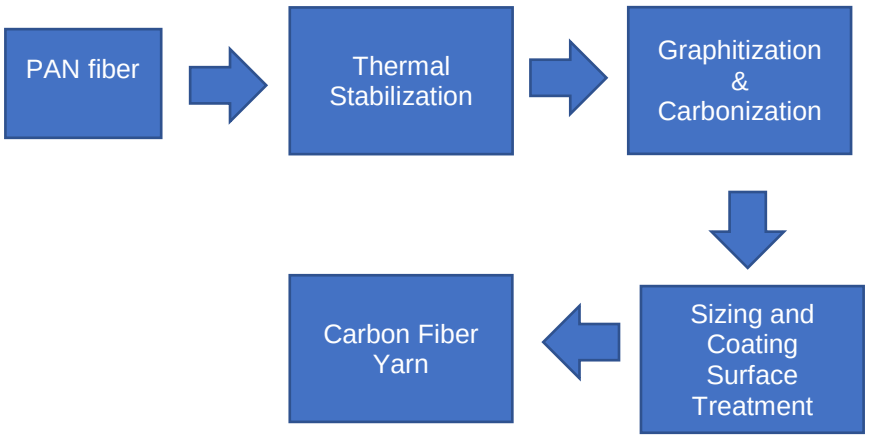

Figure 2 - Overview of carbon fiber manufacturing process

2.2 Composite Part Manufacturing Methods

The manufacturing literature review in this section is taken from the student senior project (Carlucci et al.). There are numerous methods to manufacture and mold carbon fiber parts. These techniques include vacuum bagging, resin infusion, autoclave, resin transfer molding (RTM), Sheet Molding Compound (SMC) compression molding, liquid compression molding, pultrusion, and continuous lamination to name a few. A brief description of each of these methods is given below:

2.2.1 Vacuum Bagging

Vacuum bagging composite material uses an open mold cavity. Composite material is then placed into the mold, either prepare or dry fabric that then must be wet out with epoxy. A release film is placed on top of the composite material, followed by a breather cloth, and finally by a vacuum bag film. The vacuum bag film is sealed to the mold edges using sealant tape. Once this layup is complete, a vacuum connector is installed into the vacuum film allowing a vacuum pump to pull all the air out between the mold and vacuum film. This presses the composite material against the mold cavity and pushes excess resin from the composite layup into the breather cloth, reducing the weight and increasing the strength of the final part. The part is allowed to cure and then removed from the mold where the vacuum bagging material is stripped from the part. This leaves one surface mold finished and the other relatively rough. One advantage to vacuum the vacuum bagging process is the low tooling cost and short setup time. For this specific part, a simple flat sheet of aluminum or hard plastic could be used as the tooling to create a flat plate to send to machining. A small drawback to this process is the large amount of extra material needed for each layup that must be disposed of after each part is made as seen in the below figure.

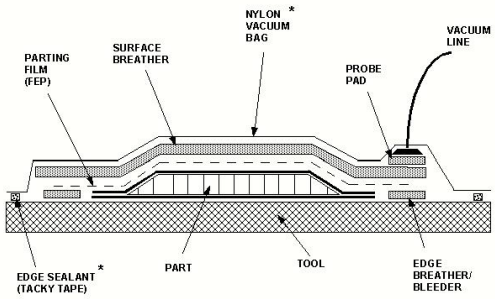

Figure 3 - Vacuum bagging setup (Carlucci et. al)

2.2.2 **Resin Infusion**

Resin infusion is a similar process to vacuum bagging except for the way in which resin is applied. In the resin infusion process, dry material is placed into an open mold and the vacuum bagging consumables are applied as in the vacuum bagging process. The only addition to this is a flow media which is placed in-between the release film and breather cloth along with a spiral-cut resin distribution tube at either end of the mold. A resin inlet is added to one side of the mold with a tube leading to mixed low- viscosity epoxy. Vacuum is then applied to the opposing side. This negative pressure pulls in epoxy which flows through the mold via the flow media, saturating the composite material. Eventually, the resin reaches the vacuum outlet where the excess is sucked up into a catch pot to prevent damaging the vacuum pump. Once the part is completely saturated, both the resin inlet line and vacuum outlet line are clamped off and the part is left to cure in the mold. This process results in a similar finished part as vacuum bagging but allows for more resin control. Resin infusion also has low tooling costs but requires more disposable materials for each part.

2.2.3 **Autoclave**

The autoclave process utilizes the same setup as vacuum bagging with one additional step. A schematic can be seen below in Figure 4. Once the composite material and vacuum bagging materials are placed in the mold, the mold is placed into an autoclave. The autoclave is a vessel that can provide large amounts of heat and pressure to the composite material on the mold. This cures the part faster, allows for a better resin to carbon ratio, and produces a stronger part. This process also yields a part with only one finished side. Like vacuum bagging and resin infusion, the tooling to for this process is very simple and can be made cheaply but a large, very expensive autoclave chamber is also required.

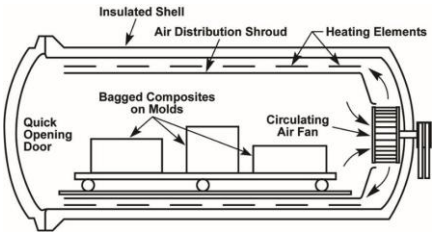

Figure 4 - Schematic of autoclave setup (Carlucci et. al)

2.2.4 **Resin Transfer Molding**

Resin transfer molding, or RTM, is a process using a rigid closed mold. First preform is draped over one half of the mold, then the other half is placed on top and the preform is compacted. Resin is then injected through gate points and replaces the air trapped between the preform layers. The air is pushed by the resin, and sucked by a vacuum at an exit gate. Once all the air has been replaced with resin the gates are closed and the preform is impregnated. After a cure phase the mold is opened and the part is removed. The RTM process has the capability to provide the best surface finish out of any of these processes. This process requires complex heated molds, making the tooling cost rather expensive and a longer lead time to have them machined.

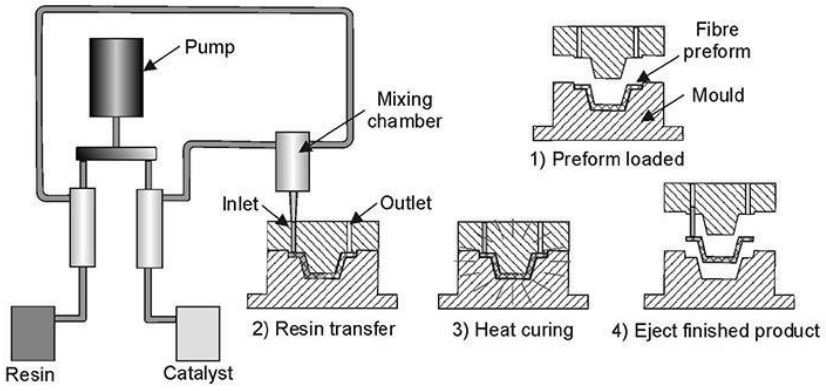

Figure 5 - Schematic of resin transfer molding process (Carlucci et al.)

2.2.5 **Sheet Molding Compound (SMC) Compression Molding**

SMC Compression molding takes carbon material mixed with resin and compresses it in a heated mold of the desired part with up to 2000 psi of pressure. After just a few minutes the mold is opened and the part is removed. The unique aspect of SMC compression molding is the carbon material that is compressed in the mold. This raw material is cheap because it is comprised of chopped fibers mixed with resin, which can even be made from breaking down old carbon parts. However, parts made with this method are not as strong due to the lack of uniform fibers running the length of the part.

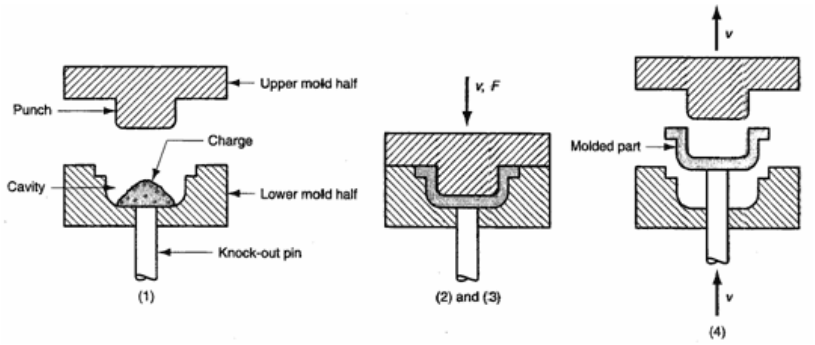

Figure 6 - Schematic of SMC process (Carlucci et al.)

2.2.6 **Liquid Compression Molding (LCM)**

Liquid compression molding or LCM is similar to SMC compression molding and yields a stronger, but more expensive part. The LCM process begins by placing 'dry' fibers into the mold. This allows the fibers to be oriented to best suit the needs of the part. Liquid resins are then catalyzed and poured over the fibers before closing the mold. Pressure is applied to ensure material is in contact with all mold areas. The mold is heated and pressure is maintained to specified levels until the part has cured. Once cured the finished part can be removed. The production time is less than a resin transfer process because there is no waiting during the injection period. The tooling required for the LCM process is less complex that the tooling for RTM yet still has substantial cost and machining time associated with it.

2.3 Composites Theory

Now that there is an understanding of composite manufacturing, we can go into the details of analysis. First, we can go through the different areas of study:

Table 1 - Composites Theory Overview (Kaw)

Area of Study	Composite Level	Visual Example
Micro-Mechanics	Fiber matrix/lamina	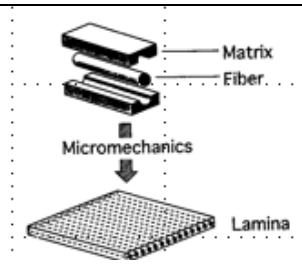
Laminate Theory	Laminate design	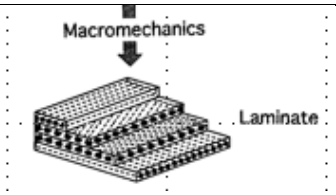
Structural Design - Mechanics of Materials - Plate and Shell Theory - FEA	Structure	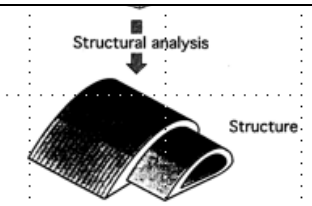

Classical Lamination Theory (CLT) is the theoretical foundation that is used to analyze composite structures. First, key terms must be identified:

Fiber – The individual carbon filaments that when bound together can create a portion of the lamina

Epoxy – The bonding material that is used to adhere multiple fiber layers together

Lamina - In composites is a single ply of carbon fiber material and epoxy.

Laminate – the bonding of lamina to each other

Composite – The ordering and bonding of lamina to create a final structure

Orthotropic – Material has 3 mutually perpendicular, orthogonal, planes of symmetry. The intersections of the planes define the principle material axes

2.3.1 **Orthotropic Lamina Mechanics**

The following is a summary of Hooke's Law for orthotropic material, used to define stress and strains at the lamina level. This is described in Barbero Chapters 1 & 2.

Starting with the expanded 3D Hooke's Law for anistropic materials:

$$\begin{Bmatrix} \varepsilon_1 \\ \varepsilon_2 \\ \varepsilon_3 \\ \gamma_{23} \\ \gamma_{31} \\ \gamma_{12} \end{Bmatrix} = \begin{bmatrix} S_{11} & S_{12} & S_{13} & S_{14} & S_{15} & S_{16} \\ S_{12} & S_{22} & S_{23} & S_{24} & S_{25} & S_{26} \\ S_{13} & S_{23} & S_{33} & S_{34} & S_{35} & S_{36} \\ S_{14} & S_{24} & S_{34} & S_{44} & S_{45} & S_{46} \\ S_{15} & S_{25} & S_{35} & S_{45} & S_{55} & S_{56} \\ S_{16} & S_{26} & S_{36} & S_{46} & S_{56} & S_{66} \end{bmatrix} \begin{Bmatrix} \sigma_1 \\ \sigma_2 \\ \sigma_3 \\ \tau_{23} \\ \tau_{31} \\ \tau_{12} \end{Bmatrix} \qquad (2.3-1)$$

The compliance matrix, [S] is symmetric and has 21 independent constants. The inverse of the compliance matrix is the stiffness matrix, [C]

$$[S] = [C]^{-1} \qquad (2.3-2)$$

Shorthand form using the compliance matrix can be rewritten as:

$$\{\varepsilon\} = [S]\{\sigma\} \qquad (2.3-3)$$

Since the lamina is orthotropic, this means that there are 3 planes of symmetry that are coincident with the coordinate planes.

For an orthotropic material, 3D Hooke's Law reduces to:

$$\begin{Bmatrix} \sigma_1 \\ \sigma_2 \\ \sigma_3 \\ \tau_{23} \\ \tau_{31} \\ \tau_{12} \end{Bmatrix} = \begin{bmatrix} C_{11} & C_{12} & C_{13} & 0 & 0 & 0 \\ C_{12} & C_{22} & C_{23} & 0 & 0 & 0 \\ C_{13} & C_{23} & C_{33} & 0 & 0 & 0 \\ 0 & 0 & 0 & C_{44} & 0 & 0 \\ 0 & 0 & 0 & 0 & C_{55} & 0 \\ 0 & 0 & 0 & 0 & 0 & C_{66} \end{bmatrix} \begin{Bmatrix} \varepsilon_1 \\ \varepsilon_2 \\ \varepsilon_3 \\ \gamma_{23} \\ \gamma_{31} \\ \gamma_{12} \end{Bmatrix} \qquad (2.3-4)$$

The equation rewritten in terms of compliances simplifies to:

$$\begin{Bmatrix} \varepsilon_1 \\ \varepsilon_2 \\ \varepsilon_3 \\ \gamma_{23} \\ \gamma_{31} \\ \gamma_{12} \end{Bmatrix} = \begin{bmatrix} S_{11} & S_{12} & S_{13} & 0 & 0 & 0 \\ S_{12} & S_{22} & S_{23} & 0 & 0 & 0 \\ S_{13} & S_{23} & S_{33} & 0 & 0 & 0 \\ 0 & 0 & 0 & S_{44} & 0 & 0 \\ 0 & 0 & 0 & 0 & S_{55} & 0 \\ 0 & 0 & 0 & 0 & 0 & S_{66} \end{bmatrix} \begin{Bmatrix} \sigma_1 \\ \sigma_2 \\ \sigma_3 \\ \tau_{23} \\ \tau_{31} \\ \tau_{12} \end{Bmatrix} \qquad (2.3-5)$$

Additionally, fiber direction would be considered transversely orthotropic, meaning that it has one axis of symmetry. This is possible, since CLT assumes that each lamina is homogenous, meaning that fibers and epoxy are randomly distributed in the transverse direction. With this assumption, 3D Hooke's law reduces to (for symmetry in the 1-axis):

$$\begin{Bmatrix} \sigma_1 \\ \sigma_2 \\ \sigma_3 \\ \tau_{23} \\ \tau_{31} \\ \tau_{12} \end{Bmatrix} = \begin{bmatrix} C_{11} & C_{12} & C_{12} & 0 & 0 & 0 \\ C_{12} & C_{22} & C_{23} & 0 & 0 & 0 \\ C_{12} & C_{23} & C_{22} & 0 & 0 & 0 \\ 0 & 0 & 0 & (C_{22}-C_{23})/2 & 0 & 0 \\ 0 & 0 & 0 & 0 & C_{66} & 0 \\ 0 & 0 & 0 & 0 & 0 & C_{66} \end{bmatrix} \begin{Bmatrix} \varepsilon_1 \\ \varepsilon_2 \\ \varepsilon_3 \\ \gamma_{23} \\ \gamma_{31} \\ \gamma_{12} \end{Bmatrix} \qquad (2.3-6)$$

The transversely isotropic equation in terms of compliances simplifies to:

$$\begin{Bmatrix} \varepsilon_1 \\ \varepsilon_2 \\ \varepsilon_3 \\ \gamma_{23} \\ \gamma_{31} \\ \gamma_{12} \end{Bmatrix} = \begin{bmatrix} S_{11} & S_{12} & S_{12} & 0 & 0 & 0 \\ S_{12} & S_{22} & S_{23} & 0 & 0 & 0 \\ S_{12} & S_{23} & S_{22} & 0 & 0 & 0 \\ 0 & 0 & 0 & 2(S_{22}-S_{23}) & 0 & 0 \\ 0 & 0 & 0 & 0 & S_{66} & 0 \\ 0 & 0 & 0 & 0 & 0 & S_{66} \end{bmatrix} \begin{Bmatrix} \sigma_1 \\ \sigma_2 \\ \sigma_3 \\ \tau_{23} \\ \tau_{31} \\ \tau_{12} \end{Bmatrix} \qquad (2.3-7)$$

Superposition can now be used to put in terms of material properties (Mello). Recall, that uniaxial stress in fiber direction is:

$$\varepsilon_1 = \frac{\sigma_1}{E_1} \qquad (2.3-8)$$

With Poisson's effects:

$$\varepsilon_2 = -\nu_{12}\varepsilon_1 \qquad (2.3-9)$$

$$\varepsilon_3 = -\nu_{13}\varepsilon_1 \qquad (2.3-10)$$

Stress in the transverse direction (2-direction) is:

$$\varepsilon_2 = \frac{\sigma_2}{E_2} \qquad (2.3-11)$$

$$\varepsilon_1 = -\nu_{21}\varepsilon_2 \qquad (2.3-12)$$

$$\varepsilon_3 = -\nu_{23}\varepsilon_2 \qquad (2.3-13)$$

Shear stress and strain are related through the in-plane shear modulus, G_{12},

$$\gamma_{12} = \frac{\tau_{12}}{G_{12}} \qquad (2.3-14)$$

A visual representation is shown below in Figure 7:

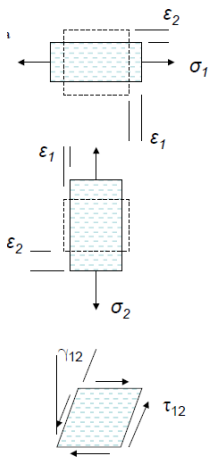

Figure 7 - Relation of stress and strain (Mello, Barbero)

For stress and strain in the 3-direction, or the thickness:

$$\varepsilon_3 = \frac{\sigma_3}{E_3} \tag{2.3-15}$$

$$\varepsilon_1 = -\nu_{31}\varepsilon_3 \tag{2.3-16}$$

$$\varepsilon_2 = -\nu_{32}\varepsilon_3 \tag{2.3-17}$$

Using superposition for the 1-direction, gives loading in 3 directions:

Loading in 1:

$$\varepsilon_1 = \frac{\sigma_1}{E_1} \tag{2.3-18}$$

Loading in 2:

$$\varepsilon_1 = -\nu_{21}\varepsilon_2 = -\nu_{21}\frac{\sigma_2}{E_2} \tag{2.3-19}$$

Loading in 3:

$$\varepsilon_1 = -\nu_{31}\varepsilon_3 = -\nu_{31}\frac{\sigma_3}{E_3} \tag{2.3-20}$$

Combining terms gives strain in the 1-direction:

$$\varepsilon_1 = \frac{\sigma_1}{E_1} - \frac{\nu_{21}}{E_2}\sigma_2 - \frac{\nu_{31}}{E_3}\sigma_3 \tag{2.3-21}$$

Doing the same in the 2 and 3-directions provides:

$$\varepsilon_2 = \frac{-\nu_{12}}{E_1}\sigma_1 + \frac{\sigma_2}{E_2} - \frac{\nu_{32}}{E_3}\sigma_3 \tag{2.3-22}$$

$$\varepsilon_3 = \frac{-\nu_{13}}{E_1}\sigma_1 - \frac{\nu_{23}}{E_2}\sigma_2 - \frac{\sigma_3}{E_3} \tag{2.3-23}$$

The terms can be substituted into the compliance matrix for orthotropic Hooke's Law:

$$\begin{Bmatrix} \varepsilon_1 \\ \varepsilon_2 \\ \varepsilon_3 \\ \gamma_{23} \\ \gamma_{31} \\ \gamma_{12} \end{Bmatrix} = \begin{bmatrix} \frac{1}{E_1} & \frac{-\nu_{21}}{E_2} & \frac{-\nu_{31}}{E_3} & 0 & 0 & 0 \\ \frac{-\nu_{12}}{E_1} & \frac{1}{E_2} & \frac{-\nu_{32}}{E_3} & 0 & 0 & 0 \\ \frac{-\nu_{13}}{E_1} & \frac{-\nu_{23}}{E_2} & \frac{1}{E_3} & 0 & 0 & 0 \\ 0 & 0 & 0 & \frac{1}{G_{23}} & 0 & 0 \\ 0 & 0 & 0 & 0 & \frac{1}{G_{31}} & 0 \\ 0 & 0 & 0 & 0 & 0 & \frac{1}{G_{12}} \end{bmatrix} \begin{Bmatrix} \sigma_1 \\ \sigma_2 \\ \sigma_3 \\ \tau_{23} \\ \tau_{31} \\ \tau_{12} \end{Bmatrix} \qquad (2.3-24)$$

From assumption number 4 in our laminate theory assumptions (plane stress), we can assume that the plate is too thin for stresses to develop in the 3-direction, therefore:

$$\sigma_3 = \tau_{12} = \tau_{23} = 0 \qquad (2.3-25)$$

Substituting (2.3-25) into (2.3-24) simplifies the strain-stress relation to:

$$\begin{Bmatrix} \varepsilon_1 \\ \varepsilon_2 \\ \gamma_{12} \end{Bmatrix} = \begin{bmatrix} \frac{1}{E_1} & \frac{-\nu_{21}}{E_2} & 0 \\ \frac{-\nu_{12}}{E_1} & \frac{1}{E_2} & 0 \\ 0 & 0 & \frac{1}{G_{12}} \end{bmatrix} \begin{Bmatrix} \sigma_1 \\ \sigma_2 \\ \tau_{12} \end{Bmatrix} \qquad (2.3-26)$$

Inverting the compliance matrix above, provides the stress-strain or reduced material stiffness matrix:

$$\begin{Bmatrix} \sigma_1 \\ \sigma_2 \\ \tau_{12} \end{Bmatrix} = \begin{bmatrix} Q_{11} & Q_{12} & 0 \\ Q_{12} & Q_{22} & 0 \\ 0 & 0 & Q_{66} \end{bmatrix} \begin{Bmatrix} \varepsilon_1 \\ \varepsilon_2 \\ \gamma_{12} \end{Bmatrix} \qquad (2.3-27)$$

Notice that it is common to use the term Q_{66} as this was its original location in the 3D equation. The terms in the material stiffness matrix are:

$$Q_{11} = \frac{E_1}{D} \qquad (2.3-28)$$

$$Q_{21} = \frac{\nu_{12} E_2}{D} \qquad (2.3-29)$$

$$Q_{12} = \frac{\nu_{21} E_1}{D} \qquad (2.3-30)$$

$$Q_{22} = \frac{E_2}{D} \qquad (2.3-31)$$

$$Q_{66} = G_{12} \qquad (2.3-32)$$

$$D = 1 - \nu_{12}\nu_{21} \qquad (2.3-33)$$

The [Q] matrix is the stiffness matrix for plane stress in material coordinates. This allows analysis for a single lamina.

2.3.2 Classical Lamination Theory (CLT)

Key assumptions in CLT (Kaw):

1. Each lamina is orthotropic
2. Each lamina is homogeneous
3. A line straight and perpendicular to mid-surface remains straight and perpendicular to mid-surface during deformation ($\gamma_{13} = \gamma_{23} = 0$)
4. The laminate is thin compared to its span (l, w, >> t) and is only loaded in its plane (plane stress, $\sigma_3 = \tau_{13} = \tau_{23} = 0$)
5. Each lamina is linearly elastic
6. No slip occurs between lamina interfaces (laminate is perfectly bonded)
7. Displacements are small compared with the thickness of the laminate

The lamina theory described in section 2.3.1 creates the basis for analyzing the laminate structure. With tensor transformation of each lamina, one can determine strains in a ply. Then stress can be determined through the $[\overline{Q}]$ matrix, and equilibrium equations are used to integrate through the laminate thickness to get stress resultants. The stress resultants are line loads and moments.

To analyze laminates effectively, transformation matrices are required to create a relationship between global coordinates and lamina principal material coordinates:

$$\begin{Bmatrix} \sigma_1 \\ \sigma_2 \\ \tau_{12} \end{Bmatrix} = [T] \begin{Bmatrix} \sigma_x \\ \sigma_y \\ \tau_{xy} \end{Bmatrix} \qquad (2.3-34)$$

The transformation matrix, [T] is:

$$[T] = \begin{bmatrix} cos^2\theta & \sin^2\theta & 2sin\theta cos\theta \\ \sin^2\theta & \cos^2\theta & -2sin\theta cos\theta \\ -sin\theta cos\theta & sin\theta cos\theta & \cos^2\theta - \sin^2\theta \end{bmatrix} \quad (2.3-35)$$

And the inverse transformation matrix is:

$$[T]^{-1} = \begin{bmatrix} \cos^2\theta & \sin^2\theta & -2sin\theta cos\theta \\ \sin^2\theta & \cos^2\theta & 2sin\theta cos\theta \\ sin\theta cos\theta & -sin\theta cos\theta & \cos^2\theta - \sin^2\theta \end{bmatrix} \quad (2.3-36)$$

Allowing for x,y stresses in terms of 1,2 direction stresses:

$$\begin{Bmatrix} \sigma_x \\ \sigma_y \\ \tau_{xy} \end{Bmatrix} = [T^{-1}] \begin{Bmatrix} \sigma_1 \\ \sigma_2 \\ \tau_{12} \end{Bmatrix} \quad (2.3-37)$$

Additionally, engineering strain must be related to tensor strain by:

$$\begin{Bmatrix} \varepsilon_x \\ \varepsilon_y \\ \gamma_{xy} \end{Bmatrix} = [R] \begin{Bmatrix} \varepsilon_1 \\ \varepsilon_2 \\ \frac{\gamma_{12}}{2} \end{Bmatrix} \quad (2.3-38)$$

Where R is:

$$R = \begin{bmatrix} 1 & 0 & 0 \\ 0 & 1 & 0 \\ 0 & 0 & 2 \end{bmatrix} \quad (2.3-39)$$

R^{-1} can be used to create tensor strain. Combining equations creates relation of strains in the 1,2 directions to the x,y directions.

$$\begin{Bmatrix} \varepsilon_1 \\ \varepsilon_2 \\ \gamma_{12} \end{Bmatrix} = [R] \begin{Bmatrix} \varepsilon_1 \\ \varepsilon_2 \\ \frac{\gamma_{12}}{2} \end{Bmatrix} = [R][T] \begin{Bmatrix} \varepsilon_x \\ \varepsilon_y \\ \gamma_{xy} \end{Bmatrix} = [R][T][R^{-1}] \begin{Bmatrix} \varepsilon_x \\ \varepsilon_y \\ \gamma_{xy} \end{Bmatrix} \quad (2.3-40)$$

Combining the [Q] matrix, (2.3-27), and transformation (2.3-37) creates a transformation of the 1,2 stress to the x,y stress:

$$\begin{Bmatrix} \sigma_x \\ \sigma_y \\ \tau_{xy} \end{Bmatrix} = [T^{-1}] \begin{Bmatrix} \sigma_1 \\ \sigma_2 \\ \tau_{12} \end{Bmatrix} = [T^{-1}][Q][R] \begin{Bmatrix} \varepsilon_1 \\ \varepsilon_2 \\ \frac{\gamma_{12}}{2} \end{Bmatrix} = [T^{-1}][Q][R][T] \begin{Bmatrix} \varepsilon_x \\ \varepsilon_y \\ \frac{\gamma_{xy}}{2} \end{Bmatrix} \quad (2.3-41)$$

Multiplying by R^{-1} changes the engineering strain to the desired relation, $[\bar{Q}]$:

$$\begin{Bmatrix}\sigma_x\\ \sigma_y\\ \tau_{xy}\end{Bmatrix} = [T^{-1}][Q][R][T][R^{-1}]\begin{Bmatrix}\varepsilon_x\\ \varepsilon_y\\ \gamma_{12}\end{Bmatrix} = [\bar{Q}]\begin{Bmatrix}\varepsilon_x\\ \varepsilon_y\\ \gamma_{12}\end{Bmatrix} \qquad (2.3-42)$$

The $[\bar{Q}]$ matrix represents coupled shear and extension. This matrix determines ply stiffness when loading is not in the principal material axes as it relates the stress-strain response for an angle ply in laminate x-y coordinates (Mello). Now strains at any point in the thickness of the lamina in terms of mid-surface strains and curvature can be written as:

$$\begin{Bmatrix}\varepsilon_x\\ \varepsilon_y\\ \gamma_{xy}\end{Bmatrix} = \begin{Bmatrix}\varepsilon_x^o\\ \varepsilon_y^o\\ \gamma_{xy}^o\end{Bmatrix} + z\begin{Bmatrix}\kappa_x\\ \kappa_y\\ \kappa_{xy}\end{Bmatrix} \qquad (2.3-43)$$

Where, κ represents the curvature or change in slopes. The last term κ_{xy}, is a twist curvature. Putting mid-surface strains into a stress-strain for any point through the thickness is done by combining with the lamina $[\bar{Q}]$ matrix:

$$\begin{Bmatrix}\sigma_x\\ \sigma_y\\ \tau_{xy}\end{Bmatrix}_k = \begin{bmatrix}\overline{Q_{11}} & \overline{Q_{12}} & \overline{Q_{16}}\\ \overline{Q_{12}} & \overline{Q_{22}} & \overline{Q_{26}}\\ \overline{Q_{16}} & \overline{Q_{26}} & \overline{Q_{66}}\end{bmatrix}_k \left(\begin{Bmatrix}\varepsilon_x^o\\ \varepsilon_y^o\\ \gamma_{xy}^o\end{Bmatrix} + z\begin{Bmatrix}\kappa_x\\ \kappa_y\\ \kappa_{xy}\end{Bmatrix}\right) \qquad (2.3-44)$$

Where k represents the ply number. Integrating across the laminate thickness, z gives the stress resultants, or plate loads, which are line loads and moments:

$$\begin{Bmatrix}N_x\\ N_y\\ N_{xy}\end{Bmatrix} = \begin{bmatrix}A_{11} & A_{12} & A_{16}\\ A_{12} & A_{22} & A_{26}\\ A_{16} & A_{26} & A_{66}\end{bmatrix}\begin{Bmatrix}\varepsilon_x^o\\ \varepsilon_y^o\\ \gamma_{xy}^o\end{Bmatrix} + \begin{bmatrix}B_{11} & B_{12} & B_{16}\\ B_{12} & B_{22} & B_{26}\\ B_{16} & B_{26} & B_{66}\end{bmatrix}\begin{Bmatrix}\kappa_x\\ \kappa_y\\ \kappa_{xy}\end{Bmatrix} \qquad (2.3-45)$$

$$\begin{Bmatrix}M_x\\ M_y\\ M_{xy}\end{Bmatrix} = \begin{bmatrix}B_{11} & B_{12} & B_{16}\\ B_{12} & B_{22} & B_{26}\\ B_{16} & B_{26} & B_{66}\end{bmatrix}\begin{Bmatrix}\varepsilon_x^o\\ \varepsilon_y^o\\ \gamma_{xy}^o\end{Bmatrix} + \begin{bmatrix}D_{11} & D_{12} & D_{16}\\ D_{12} & D_{22} & D_{26}\\ D_{16} & D_{26} & D_{66}\end{bmatrix}\begin{Bmatrix}\kappa_x\\ \kappa_y\\ \kappa_{xy}\end{Bmatrix}$$

Where,

The extensional stiffness is

$$A_{ij} = \sum_{k=1}^{n} \overline{(Q_{ij})}(z_k - z_{k-1}) \qquad (2.3-46)$$

The bending-extension coupling stiffness is

$$B_{ij} = \frac{1}{2}\sum_{k=1}^{n}\overline{(Q_{ij})}(z_k^2 - z_{k-1}^2) \qquad (2.3-47)$$

And the bending stiffness is

$$D_{ij} = \frac{1}{3}\sum_{k=1}^{n}\overline{(Q_{ij})}(z_k^3 - z_{k-1}^3) \qquad (2.3-48)$$

In which *k*, is the layer number, *n* is the total number of layers, and *z*, is the distance from the mid-plane of the laminate to layer of interest.

Shorthand for this relation is written as:

$$\begin{Bmatrix} N \\ M \end{Bmatrix} = \begin{bmatrix} A & B \\ B & D \end{bmatrix}\begin{Bmatrix} \varepsilon \\ \kappa \end{Bmatrix} \qquad (2.3-49)$$

The ABD matrix is the backbone of shell elements, which are typically used to analyze laminate structures (Mello).

2.4 Finite Element Analysis

Finite Element Analysis (FEA) or Finite Element Method (FEM) is a procedure to numerically analyze structures. These tools are typically used for solving complex problems that cannot be simplified or solved adequately with classical methods. Common areas of use are in stress analysis, fluid flow, and heat transfer. It is important to note that numerical methods are approximations of the actual system and are not exact solutions. Understanding the mathematical model, assumptions, element type, and proper meshing can make FEA a viable way to solve complex problems. However, FEA can be quick to provide an inaccurate approximation and this is where engineering judgment and understanding is required to validate results. In this case, Abaqus® software is being used to analyze the complex material structure in order to better understand displacement due to loading.

As described above, the use of FEA software requires the user to understand key assumptions about the model to ensure correct modeling is used. The author experienced difficulty (as most FEA users do), while trying to improve modeling. Some areas of difficulty were in refining the mesh to properly define the complex geometry. Additional areas were in modeling contact for bend testing, element selection, and proper partitioning.

The figure below shows the process flow of the Abaqus® FEA software. The steps within the process flow are further described in subsequent sections.

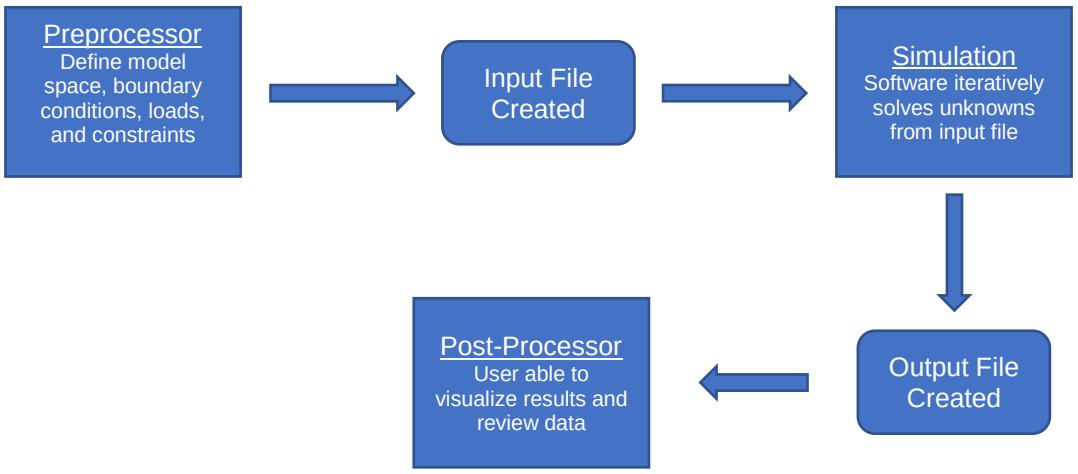

Figure 8 - Overview of FEA software

2.4.1 **Preprocessor**

The preprocessor is a graphic environment that lets the user create the physical problem. In Abaqus® the user can create their own part and define geometry, or a model can be imported. Both methods were used in this research. For the thin plate analysis, geometry was created in the preprocessor environment. This provided an efficient way to create simple geometry. For the complex part, a model was created in Siemens NX and de-featured for simplicity in the FEA environment.

Before creating parts, the user needs to fully understand the problem they are trying to solve and what assumptions are applicable from engineering theory. Use of the proper model and assumptions will allow the user to produce accurate simulations. Additionally, understanding the problem can allow the user to take advantage of more computationally efficient simulations. It will

also drive the modeling space, geometry choice, and type of part used in the preprocessor. In general, the following steps are used in the preprocessor environment.

1. Create part geometry – Import or create part geometry

   Requires the user to define the type of problem they are trying to solve. User can choose 2D or 3D geometries. Within those modeling spaces the user can then choose the type of part they would like to create: deformable, discrete rigid, analytical rigid, or Eulerian. The user then needs to define the base feature. In this research, both solid and shell models were used to create geometry.

2. Define the material

   Create material and define the properties of the material. The user must know basic engineering properties of the material they are studying. For the initial models, isotropic material properties were used to create a baseline model. The model was then made increasingly complex by changing properties to advanced material properties requiring engineering constants in 3D space.

3. Create Section Assignment

   User must define part section assignments. The section assignments are then linked to material properties, which become section properties. This allows for complex parts that have unique properties in different areas of the model. For this research, the section properties were the same across the entire part. Note that this is not a homogenous assumption as material properties in the advanced materials varied in coordinate direction.

4. Create Assembly

   A part is added to an assembly through the instance process. This allows the designer to create assembly constraints and linkages if multiple part interactions are being analyzed. This type of interaction was modeled in the 3-point bend simulations.

5. Create Step

   A step is required to define a change to the conditions of the model. In this module, the user defines the analysis step or steps. It allows the designer to create constraints,

changes in boundary conditions, or changes in loading. Additionally, it allows the user to request output information during analysis.

6. Create Interactions

   For problems requiring the analysis of multiple parts, objects, or constraints, the user can specify interactions between parts or geometries. In the 3-point bend analysis, a constraint was used to simulate the roller contact with the part during testing.

7. Define Loading and Boundary Conditions

   Boundary conditions define the restrictions placed on the model and allow for the simulation to be solved. The user defines conditions and degrees of freedom within the model. Additionally, the designer defines the loading condition of the part to drive simulation of the problem.

8. Define the mesh and select element type

   The part mesh defines the elements and nodes used in the part for solving the system of equations in the simulation. Understanding the areas of interest are critical to the meshing process as the user may need to control mesh density, element shape, and element type. The software can automatically choose elements based on geometry, however the user needs to understand what is chosen and why in order to improve simulation accuracy.

9. Create and Submit Job

   The final step in the preprocessor is to create and submit the job. The job is created in this module and can be checked prior to submission. It is highly suggested to check the job prior to submitting. The software checks the user input file and looks for errors that can lock up the simulation. Checking the file is useful to save time on processing time of jobs that may have input files that require improvement in order to result in a converged solution.

2.4.2 Simulation and Post-Processing

The output of the preprocessor is an input file that is used to run the Abaqus® simulation. The simulation solves the problem through the iterative process described in section 2.4.2. If the model converges to a solution, then the post-processor can be used to visualize the results. It also allows the user to troubleshoot modeling or simulation errors. In the post-processor, the user can manipulate the model to see visual representations of engineering analyses including stress, displacement, rotation, among other areas of interest. In cases of this study, the displacement is the primary motivation for analysis.

2.4.3 Basic Finite Element Theory

In FEM, a structure is discretized into a body of small elements. The elements are used to simplify complex geometry and thus make it easier to analyze. Each element contains nodes that can have rotational degrees of freedom, as well as displacement. The elements are joined by shared nodes. Shape functions are used to approximate the values in-between nodes by interpolation of nodal values. Shape functions are also referred to as interpolation functions. Loads and boundary conditions are used to form the matrix equation:

$$\{F\} = [K]\{d\} \qquad (2.4-1)$$

Where [K] is the global stiffness matrix of the system, {d} is the nodal displacement vector, and {F} is the nodal force vector. The global stiffness matrix is the sum of the stiffness matrices of the individual elements, [k]. In order to solve for the unknown nodal displacements, the global stiffness matrix is inverted. Boundary conditions in the global stiffness matrix make the matrix non-singular so that it can be inverted:

$$\{d\} = \{F\}[K]^{-1} \qquad (2.4-2)$$

However, in most complex systems there are many unknowns making inverting the [K] matrix inefficient. Instead, Abaqus® uses algorithms based on user input to solve the matrix equations with Newton's method or other iterative mathematical methods to improve the speed to solution (Abaqus).

3 FIRST ORDER MODELS

3.1 Beam Theory Analysis and Plate Theory Modeling

To better understand the system and expected results, the part model was simplified to a more basic form. This allows for validation of theory, and expected results which contributes to improved confidence in engineering models once additional complexity is added. In general, the part is thin, with a large span (length > width >> thickness). Additionally, one end of the part is fixed and the other is loaded perpendicular to the part. This lends itself well to beam theory for a simplified validation. However, the part itself is not a beam as the length is greater than width by an order of 5. For beam theory to be properly used, the part length would need to be much greater than both the width and thickness. Knowing the limitations of the theory, models were created for plates of various widths and lengths. The models were run as 3D plates in FEA and results were compared to oversimplified beam theory approximations. This was done to create a baseline understanding of the plate deflection as beam theory would still be expected to be on a similar order to the plate model.

Starting with classical beam theory as the most fundamental model the following key assumptions are necessary (Young):

1. The beam is homogeneous
2. The beam is straight
3. Cross-section is uniform
4. Beam is symmetric in longitudinal plane
5. All loads and reactions are perpendicular to beam axis, and lie in the same plane
6. Beam is long in proportion to its thickness (span/depth ratio > 8)
7. Beam is not disproportionately wide (This assumption was not met with the geometry used)

To meet the other key assumptions, the system was simplified as follows:

1. 6061 aluminum used as material to satisfy assumption 1 (actual part is non-homogenous)
2. Uniform rectangular cross-section created (actual part has non-uniform cross section)

3. Assumption 7 is not satisfied, but results still used to compare to FEA model as a baseline approximation

With beam theory assumptions, the width of the actual plate was ignored. This allowed the 1-D beam's maximum displacement to be approximated by simple math. **Error! Reference source ot found.** below shows the equation for finding max displacement of a cantilevered beam with a point load at the tip (Young).

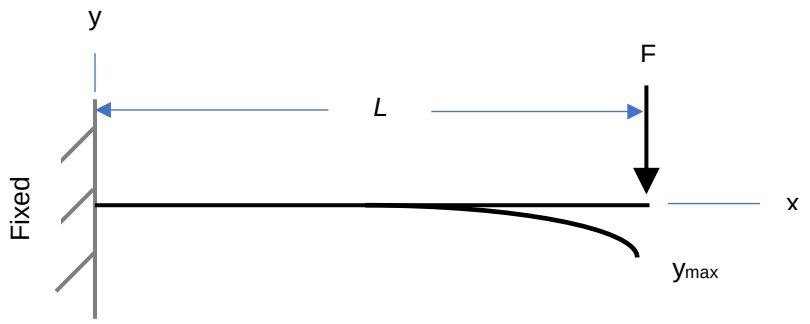

Figure 9 - Cantilever beam

$$y_{max} = -\frac{FL^3}{3EI} \qquad (3.1-1)$$

The actual basic models were thin plates of varying lengths and widths. The thickness remained constant in each study and results are compared to beam theory as a baseline comparison. These models were created as 3D deformable solids. Aluminum was chosen as the material since it is a common manufacturing material. For the models, 3D stress elements were used. They were C3D8R, which are 8 node linear bricks with hourglass control and reduced integration. Additionally, the mesh through the thickness of the plate was controlled to ensure a minimum of 2 elements were used through the part thickness. It is widely known that multiple elements through the thickness are required to get accurate solutions as max tension and compression in bending occur at the top and bottom of the part. Without creating multiple elements, the model has the risk of "locking" which can create overly stiff elements, thus incorrectly predicting deflection. Therefore, multiple elements required to discretize the stress variation occurring through the part thickness.

Each plate model was setup with the following boundary conditions:

1. Entire thickness at the part origin is fixed along the width of the part

   Fixed displacement: $u_1, u_2, u_3 = 0$

   Fixed Rotation: $ur_1, ur_2, ur_3 = 0$

2. Concentrated point load of 0.392 N at cantilevered end of plate. The concentrated load is in the center of the width of the plate

The boundary condition and loading setup can be seen below in Figure 10.

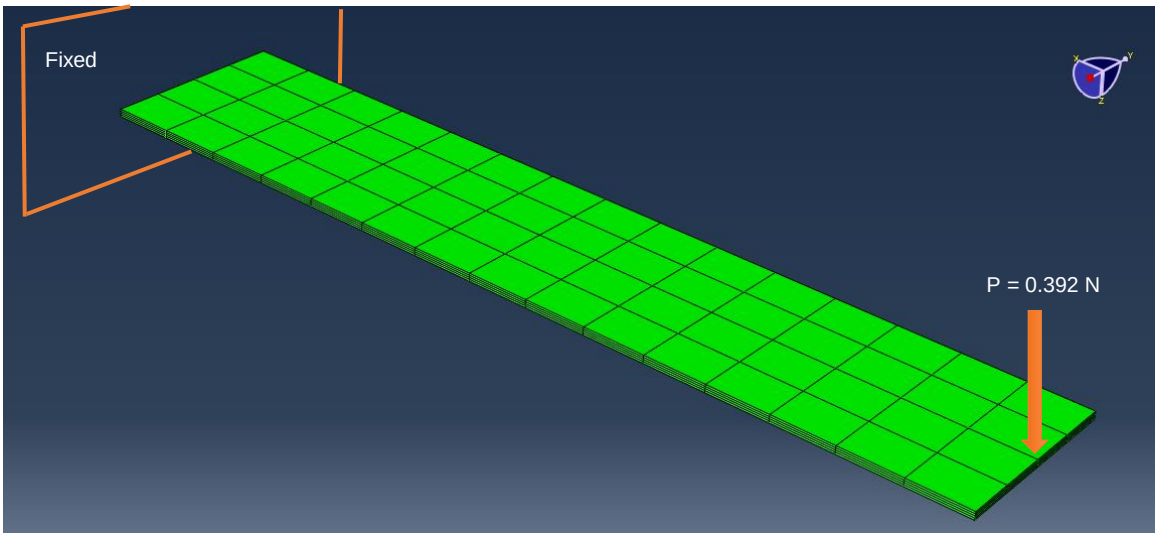

Figure 10 - Boundary conditions for plate model

The maximum deflection of each plate was then analyzed and recorded. The results were compared to the beam theory approximation as a baseline check. Figure 11 below is an example of analysis performed for the 340mm by 60mm plate. As you can see, there are 4 elements through the thickness of the part. The image shows the maximum deflection in the z-direction. Since the concentrated force is through the centerline of the width, the only deflection expected is in the z-direction. In this specific analysis, a mesh of 400 nodes and 240 elements was created.

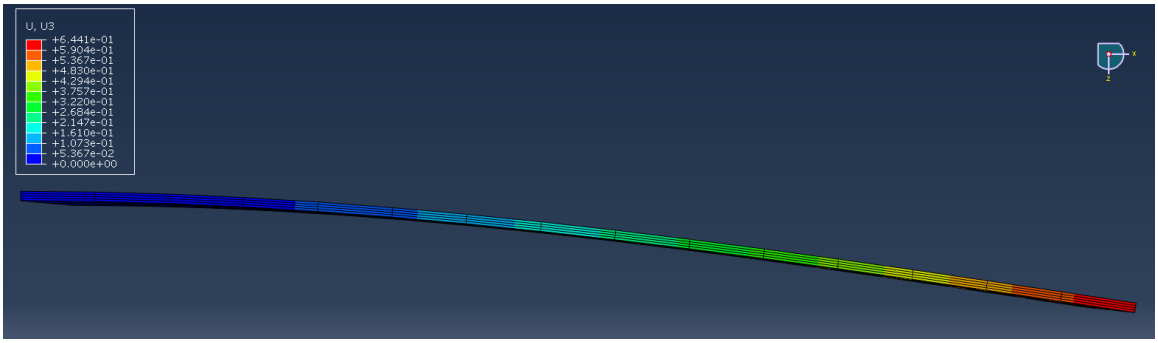

Figure 11 - Analysis of 340mm x 60mm x 2.5mm plate

With sample plate modeling and analyses completed, the results were compared. As can be seen in the table below, the results of the plate bending were very similar to the analytical beam theory approximations. This is not entirely surprising as the plates were point loaded in the y-axis plane of symmetry. This loading condition meant that there was no twist in the xy-plane. The results would be much different for a part not loaded in the plan of symmetry. Additionally, the results would likely be closer to beam approximation solution if mesh were further refined. However, the mesh density and results are within expectations for this study.

Table 2 - Results of Beam and Plate Analyses. Aluminum used with E = 68.9 GPa

Length L, [mm]	Width b, [mm]	Nodes	Elements	Second Moment of Inertia I, [mm^4]	Beam Theory Max Deflection (Analytical) δ_{max}, [mm]	Plate Theory Max Deflection (Abaqus® Model) δ_{max}, [mm]	Difference (Beam vs. Plate) %
100	20	165	80	26.0417	0.07282	0.07328	0.63%
100	60	225	128	78.125	0.02427	0.02346	-3.36%
300	60	360	184	78.125	0.6266	0.6071	2.50%
340	60	400	240	78.125	0.65542	0.6441	1.73%

3.2 Benchmarking and Calibration

With the plate model working as expected, the next step was to build upon the basic model. A carbon fiber epoxy laminate was designed, built, and tested. Laminates were built up using a LCM molding process to create approximately a 6-inch by 6-inch by 0.1-inch composite plate. The

lamina consisted of $[W_{0/90}, 0_2, W_{0/90}]_s$ layup. The unidirectional fiber is Toray T700, while the cloth was 0/90 fiber from CST Sales catalog. Fibreglast 2000 series epoxy was used. The coupon was then cut into approximately 4-inch by 0.45-inch by 0.1-inch samples. These samples were used for 3-point bend testing. The 3-point bend test is an ASTM standard that allows one to figure out material properties from an orthotropic part. Essentially a part is put on 2 rollers and a load is applied to the center of the part. The applied force and deflection are recorded using data acquisition software. This provides the basis for determining material properties of the composite. In this case, the ideal method to determine properties would have been to build up coupons of a single material type. The ASTM standard assumes that all material in the laminate is the same. However, due to time constraints on the project, coupons were made using both the unidirectional fiber and cloth weave consisting of 0/90 directional fiber.

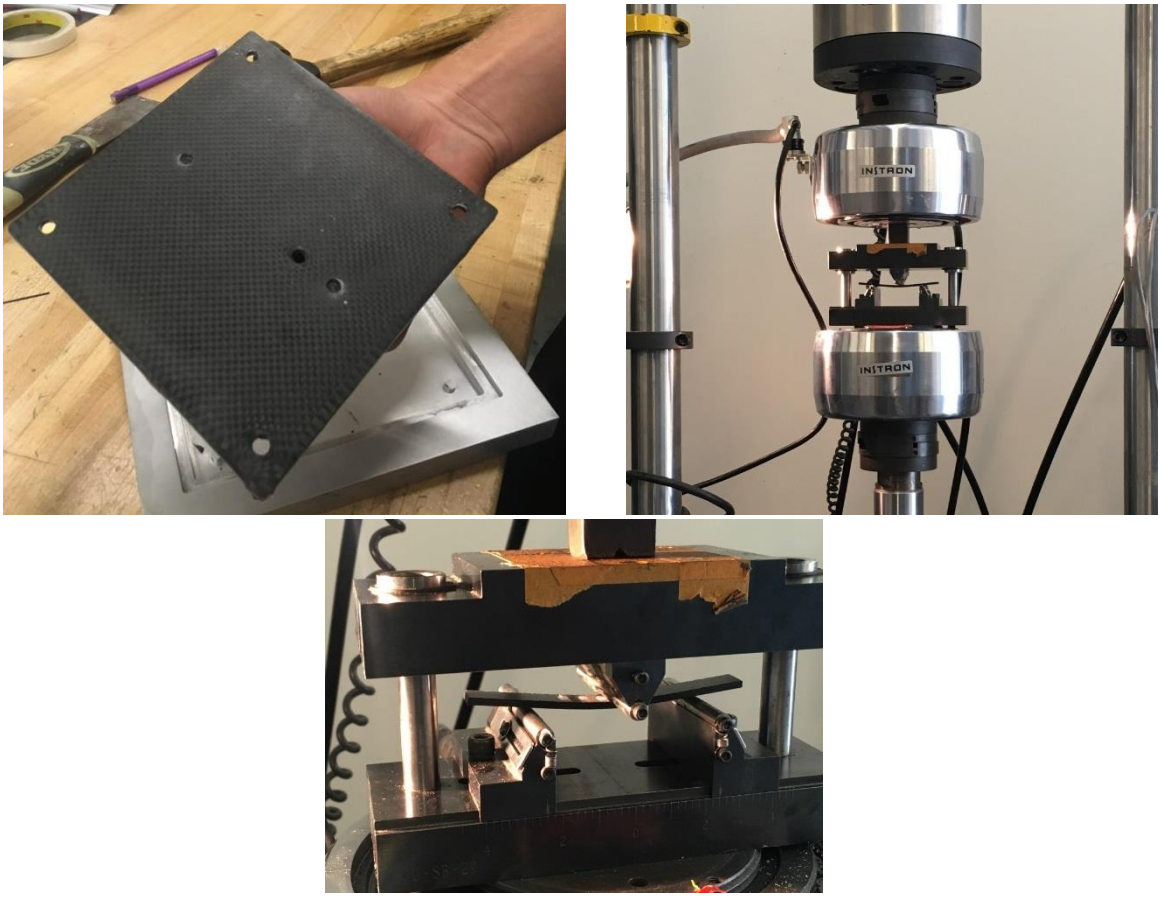

Figure 12 - 3-point bend Testing. Upper left shows a plate manufactured by students. Upper right is instron bend test, and bottom is a close-up of bend test setup.

A total of 5 coupons were tested on an Instron 1331 tester with modified fixturing to perform the 3-point bend test. Initial settings for the Instron were 200lb/Volt, a travel of 0.001" per second, and 2 scans/second. However, the parameters were tuned after the first test to travel 0.002" per second and 3 scans/second for better data capture. The length, width, and thickness of each coupon was measured prior to trial. A summary of initial coupons is shown below in Table 3 - Coupon measurements for 3-point bend test.

Table 3 - Coupon measurements for 3-point bend test

Coupon	Length	Width [mm]				Thickness [mm]			
	L [mm]	W_1	W_2	W_3	W_{avg}	t_1	t_2	t_2	t_{avg}
1	3.99	0.45	0.45	0.45	0.45	0.1	0.1	0.1	0.1
2	3.99	0.46	0.46	0.46	0.46	0.1	0.1	0.1	0.1
3	3.99	0.46	0.45	0.44	0.45	0.1	0.1	0.1	0.1
4	3.99	0.46	0.47	0.47	0.467	0.1	0.1	0.1	0.1
5	3.99	0.45	0.45	0.45	0.45	0.1	0.1	0.1	0.1

The average coupon size was then created in Abaqus® as the baseline for the 3-point bend simulated model. The laminate was modeled as a mid-plane, shell element model. This is a common approach to model thin plates. To aid in modeling, the plate was partitioned into 8 areas. Partition lines were created through the longitudinal center of symmetry on the part. Additionally, they were created through locations where support rollers were simulated, as well as through the geometric center of the part along the transverse axis. In order to simulate the rollers, the following boundary conditions were created:

1. Rollers supporting the plate were constrained prevent z-axis displacement ($u_3 = 0$)
2. The center point of the plate was constrained to only move in z-direction (u_1, $u_2 = 0$)

These boundary conditions were created along their corresponding partition lines.

To simulate the roller applying the force to the plate, an additional partition was added on each side of the x-axis mid-point of the part. The roller was assumed to be 0.2" wide and thus a partition of 0.1" was created on each side of the center line. A reference point was then created

above the plate in the center of the part. This reference point would be used to both create a constraint simulating the roller force, and provide a point for history output requests for

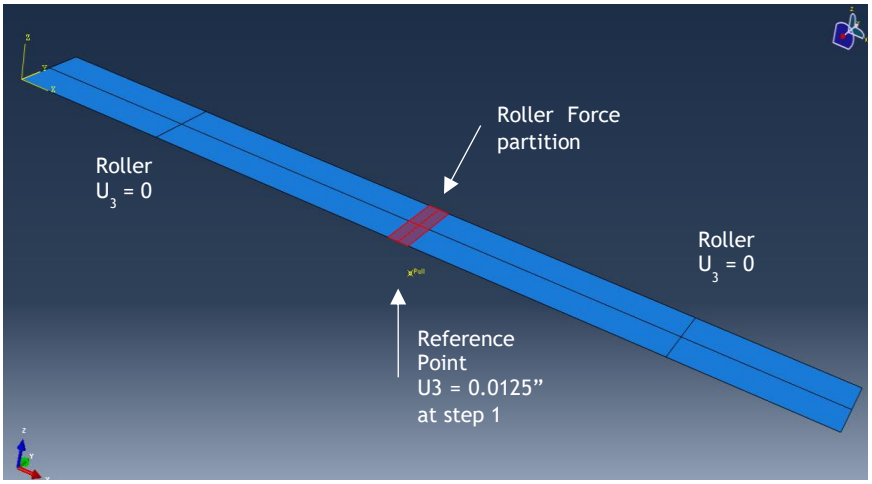

Figure 13 - Boundary conditions for 3-point bend simulation in Abaqus®

displacement and force. An equation constraint was used to tie the reference point to the roller impact location. The equation used stated that if reference point displacement moves, then the center partition on the plate must move by the same distance. This forced interaction created a simple way to request reaction forces and displacement field outputs to be used for creating a simulation force displacement curve. The loading condition for the part was a displacement of 0.125” through the reference point, thus forcing the plate to move 0.125” in the partition location. **Error! Reference source not found.** shows the visual representation of the boundary conditions and loading.

The initial model was ran using material property baseline data, which assumed 60% fiber volume. The force-displacement results were exported from the Abaqus® history output so that the results could be compared to the experimental data. The 60% fiber volume baseline proved to be too stiff as the force required to displace the part 0.125” was more than double the experimental results of approximately 80 lbs. Based on these results, the fiber volume was scaled to 30%, which is a reasonable assumption for experimental layups and molding. However, the 30% fiber volume deflection was still too stiff. Finally, the part material properties were tuned to match the

experimental force-displacement curves. The values for tuned properties were approximately 30% fiber volume for unidirectional fiber and 25% fiber volume for the cloth.

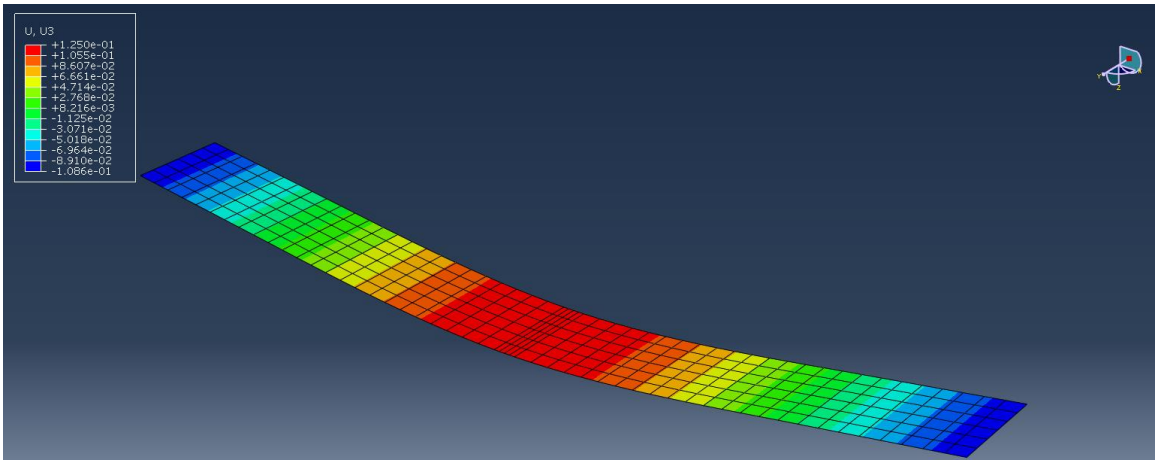

Figure 14 - 3-point bend test modeled in Abaqus®. Mid-plane shell element model with 312 S4R elements and 371 nodes

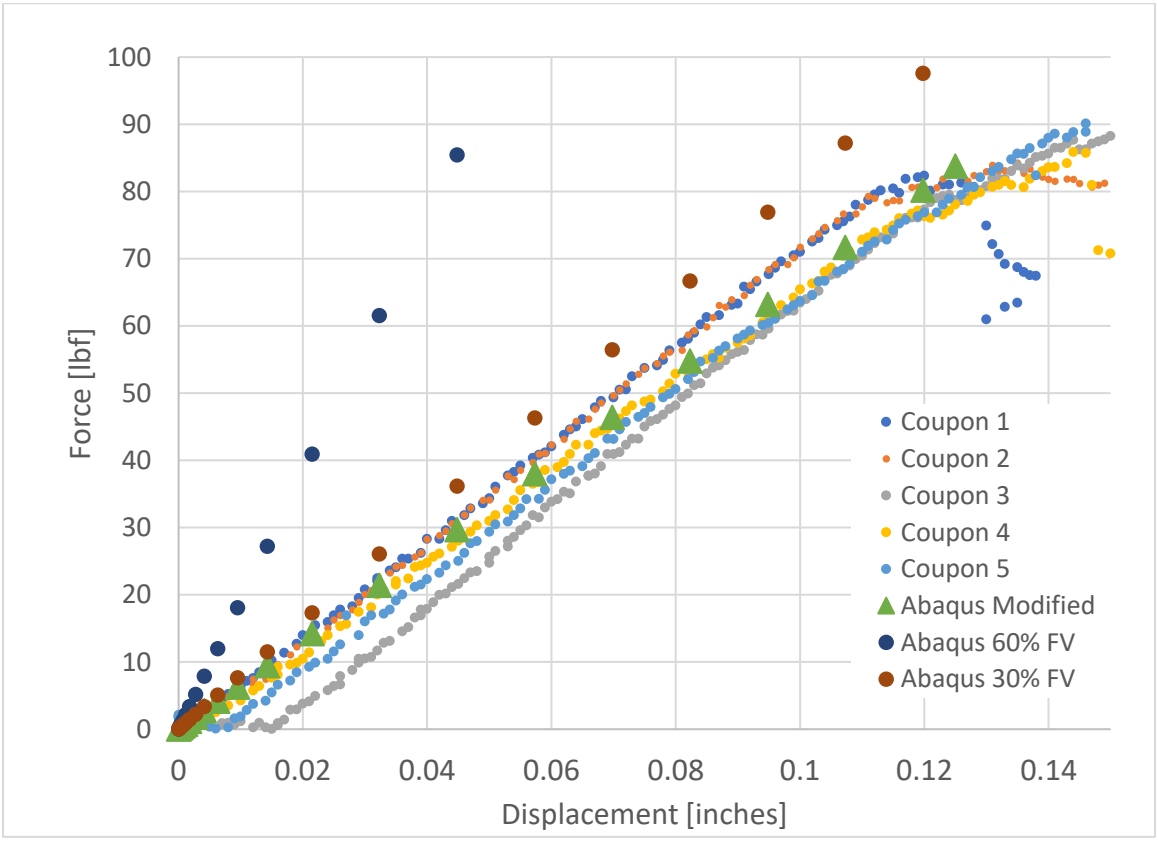

Figure 15 - Experimental data compared to finite element model

4 FINAL PART MODELING AND OPTIMIZATION

4.1 Model Description

4.1.1 Geometry, Loads, and Boundary Conditions

With representative material properties determined, the final part can be modeled. The complex part is asymmetric and slots, and holes resulting in a non-uniform part. This makes modeling and manufacturing more difficult than the baseline models. The part, boundary conditions, and loading is pictured below in Figure 16.

The part is roughly defined by length, L; width, w, and thickness. The length of the part is 340mm, width is 62mm, and thickness is 2.5mm. To simulate the use case of the part, a section of the part is fixed as it would be in the assembly. However, the bolt holes shown were not constrained, instead the surface was partitioned and entire area fixed. This approximation was used as this is how deflection on an actual part is experimentally tested. This reduced complexity in FEA analysis and made it simpler to compare to experimental results.

Boundary conditions for the part are as follows:

Fixed portion of part:

$u1 = u2 = u3 = 0$

$ur1 = ur2 = ur3 = 0$

A concentrated force of 0.392N acting in z-direction as shown below.

Figure 16 - Boundary conditions of prototype part

4.1.2 **Element Type, Mesh**

Element selection is critical to simulation results. Typically, geometry, and the type of problem the user is trying to solve drive element selection. For this project, multiple elements were investigated to determine best approach for modeling.

Conventional Shell elements discretize a reference surface through definition of the shell element's planar dimensions. These elements are used for problems where thickness is significantly smaller than the other dimensions, such as this complex part. Since conventional shell elements are based from a planar shape, the user will need to define the plane. This shape is typically defined as mid-plane, meaning that the elements are selected in the mid-section of the plane of interest. There are 6 degrees of freedom for conventional shell elements: x, y, and z displacement, as well as x, y, and z rotation. For the complex part, the thickness of the model was removed to create a planar model. The thickness was then defined by the composite laminae (Abaqus).

Brick elements are part of a family of continuum elements. These types of elements are also called solid elements as they discretize an entire model in 3D space. This is often the element of choice for 3D stress problems as it can define many surfaces, shapes, and envelopes. Since it is in 3-D space, the faces of each element can easily build upon each other. This is similar to bricks in a building in that each brick adds a layer to the structure and can be moved, stacked, or rotated to define a unique shape. Brick elements have 3 degrees of freedom for displacement in x, y, and z directions (Abaqus).

Continuum Shell elements are based from conventional shell elements, but are similar to 3-D brick elements in that they discretize the entire model in 3 dimensions. However, the continuum shells are defined such that the kinematic and constitutive relationships within nodes and elements resemble the conventional shell element. The continuum shell element has degrees of freedom in x, y, and z displacement only. Since these elements are discretizing through the part thickness, they can be used to better predict the effect of transverse shear, which could lead to thickness change (Abaqus).

Partitioning a part is a common practice used to isolate areas of interest, define constraints, or connections, nodes, and to refine or improve mesh quality in important regions of the model. Examples of partitioning is shown in Figure 17 and Figure 10. The example of the 3-point bend test shows partitioning used to define contact locations of applied force. It also shows partitioning to define geometry constraints. The center point is used as a boundary condition to restrict motion of the very center point of the part to only the z-direction. The intersection of the partition defines nodal geometry of the part. Without the partition, it would be difficult to define the center of the part as the mesh sizing could vary such that a node is not in the center of the part.

In the final part, multiple partitions were created. The first partition was created to define the fixed loading area of the part. A similar partition was created at the tip of the part to refine mesh in the loading area. The other features in the part such as the holes and slots had partitions created near them to drive mesh quality improvements. Partitioning around the holes and slots lets the user create a more refined mesh in those areas and provides a transition to the rest of the part. The additional benefit is that the model can be more computationally efficient as there are fewer elements in areas that do not require such fine meshing.

Figure 17 - Partitioning of prototype part

With 6 major sections of the part defined, the mesh could be created. The fixed area also contained holes that had smaller partitions to control element quality around the holes, but in

general this will be referred to as the fixed area. A structured mesh was created to define quadrilateral elements in the largest area of the part. The shape of this area was not entirely prismatic, so the structured mesh helped to drive a mesh shape that kept quadrilateral element shape. Using the standard mesh seeding controls in Abaqus® resulted in a “growing” mesh that

has non-uniformities in the center of the part due the unique part shape. The unstructured mesh created elements that gave errors when modeling from non-linearity. The areas around the slots and holes also used structured meshing in attempts to define the hole with approximately 16 nodes. With improved meshing, the stress distribution is more uniform and results are more accurate. The final meshed part contained 880 shell elements with a total of 985 nodes.

Figure 18 - Meshing examples of prototype part

4.1.3 **Lamina Material Properties**

The complex part is approximately 2.5mm thick, which correlated well to 12 layers of unidirectional web material or 6 layers of weave. There were two prototypes created by the team and an additional model created as a study for a higher stiffness model.

For the prototype parts, unidirectional Toray 700 SC fiber was used in conjunction with ±45 weave. The weave was catalog material purchased from Fibreglast, 3K plain weave. The parts used Fibreglast 2000 epoxy as the resin. Since the 3-point bend testing was performed on the same material, properties were estimated based on the results of the tests.

Additionally, a high modulus part was modeled and compared to previous studies. The material for the high modulus study was Toray M46J. The results of this testing were compared to Toray M40J experimental testing. Properties for all lamina studied are summarized in the table below. Note that the E1 modulus is dominant in the loading for this study, and properties were linearized from experimental testing. Further testing would be necessary to further validate the transverse properties.

Table 4 - Material properties for lamina used in analysis. Note unidirectional material and cloth have volume fractions of approximately 30% based on testing. M46J and M40J assumed volume fraction of 60%.

Property	Unidirectional Fiber Epoxy Lamina (Toray 700 SC / Fiberglast 2000) ~30% volume fraction	±45 Cloth Fiber Epoxy Lamina (Weave/Fibreglast 2000) ~30% volume fraction	Toray M46J Unidirectional Lamina (M46J/Toray Epoxy) 60% volume fraction	Toray M40J (Provided by Customer for laminate) 60% volume fraction
E1 [GPa]	62.05	20.684	246	237.87
E2 [GPa]	4.826	20.684	7.1	10.342
E3 [GPa]	4.826	13.789	7.1	10.342
v1	0.28	0.05	0.3	0.28
v2	0.28	0.05	0.3	0.28
v3	0.05	0.3	0.5	0.28
G1 [GPa]	2.758	1.723	3.05	6.894
G2 [GPa]	2.758	1.723	3.05	6.894
G3 [GPa]	1.379	1.723	2.07	6.894

4.1.4 **Laminate Definition**

Two different layups were chosen for the prototypes. This was done to provide additional variables to validate the model. With multiple layup types, the models could be validated as to accuracy of predicted deflection. For the first prototype, the layup was $[0_2/(W_{\pm 45})_2]_s$. The second prototype part used a layup with weave at the top, middle, and bottom, and unidirectional fiber sandwiched between weave layers. The layup for prototype 2 is $[W_{\pm 45}/0_2/ W_{\pm 45}]_s$. For the M46J layup, 12 layers of unidirectional fiber, $[0_{12}]$ were used.

Understanding the loading case for the physical model gives engineering intuition into the relative deflection expected in each model. Since the part is primarily in bending, the laminate bending stiffness matrix, [D], is the primary contributor in the stress-strain relationship. Additionally, understanding that the maximum stresses in pure bending are at the top (max tension) and bottom (max compression) of the thickness of the part. Therefore, the E1 modulus on the top and bottom of the part is the primary factor of part stiffness. Table 5 below shows cases, layups, and relative predicted deflection.

Table 5 - Laminate definitions for finite element modeling

Case	Prototype 1	Prototype 2	M46J
Layup	$[0_2/(W_{\pm 45})_2]_s$	$[W_{\pm 45}/0_2/ W_{\pm 45}]_s$	$[0_{12}]$
Visualization of Layup	Uni (0) Uni (0) W (±45) W (±45) W (±45) W (±45) Uni (0) Uni (0)	W (±45) Uni (0) Uni (0) W (±45) W (±45) Uni (0) Uni (0) W (±45)	Uni (0) Uni (0) Uni (0) Uni (0) Uni (0) Uni (0) Uni (0) Uni (0) Uni (0) Uni (0) Uni (0) Uni (0)
Predicted Deflection	Moderate	Most	Least

4.2 Modeled Results

4.2.1 Prototype 1 Results

The first prototype was modeled using a mid-plane conventional shell model. The mesh was consistent across all models as were the elements chosen. All models used S4 shell elements, which are 4 nodes per element. On the final part, there were 880 elements and 985 nodes. This prototype is expected to deflect less than prototype 2 as the unidirectional fiber was placed in locations of maximum stress. The unidirectional fiber has a higher modulus, therefore given the same loading it would be expected to deflect less than prototype 2. Deflection in the z-direction is shown for the part as it is far greater than deflection in the other directions. The magnitude of deflection is nearly identical to z-direction deflection. For this part, the maximum displacement was predicted to be 1.224 mm or 0.048 inches.

Figure 19 - Prototype 1 deflection results

4.2.2 Prototype 2 Results

The second model created was for prototype 2. Again, the mesh and elements are the same as in prototype 1 (880 S4 elements, 985 nodes). The expected deflection for prototype 2 model is greater than prototype 1 since the weave was put at the top and bottom of the part. The modeled displacement for prototype 2 was a maximum of 2.428 mm or 0.0955". This aligns to the expected results based on modulus differences between the unidirectional fiber and the weave.

Figure 20 - Prototype 2 deflection results

4.2.3 Future High Performance Part

Lastly, a potential future high performance part was modeled. The part was modeled with 12 layers of M46J unidirectional fiber. Material properties were taken based on datasheets, and assumed epoxy properties. This part is expected to be much stiffer than the prototypes since its E1 modulus is 4x greater than the prototype parts. However, in practice, a few layers of weaver are likely necessary as the part would not be difficult to manufacture and handle without strength in the transverse directions. Meshing and element selection was consistent with both prototype models. The maximum predicted deflection based on the FEA model is 0.3785mm or 0.014". This meets the success criteria of the design. With the unidirectional material only, the twisting of the

part due to loading can be seen in the displacement map below. In the other parts, the 45º weave prevented rotation.

Figure 21 - High performance part deflection results

The M46J predicted model was then compared to 3rd party analysis that the customer had performed on M40J material. The 3rd party FEA analysis was performed using Siemens NX. The part analyzed was more complex than the prototype parts, but shares very similar geometry. Additionally, the 3rd party model appears to have used continuum brick elements instead of shell elements. The predicted deflection of the part with M40J material is 0.438mm. This is approximately 15% greater than the M46J deflection. However, the modulus for M46J material is 16% greater than M40J. Based on these analyses, it is believed that the mid-plane shell element

4.2.4 **Modeled Results and Experimental Results**

The modeled parts were compared to experimental deflection of prototyping using testing that involved fixing the end of the part, measuring as-cantilevered height, and then adding weight to measure loaded deflection.

The results are shown below in Table 6. Both the M46J and Prototype 1 model align well to experimental results. It is believed that Prototype 2 should be retested to validate deflection. The results of this testing are discussed in more details in Chapter 6.1.

Figure 22 - 3rd party analysis of M40J layup

Table 6 - Modeled and experimental deflection. Further discussion found in results Chapter 6.1.

Part Layup	Model Deflection	Empirical Deflection	% Difference	Comments
M46J model $[0_{10}]$	0.3785mm	Compared to M40J similar part, 0.438mm	13.5%	Aligns to difference between Moduli in M46J and M40J
Prototype 1 $[0_2 / (W_{\pm 45})_2]_s$	1.224 mm (0.048”)	0.049”	2.0%	Well correlated, but limited data
Prototype 2 $[(W_{\pm 45})/0_2 /(W_{\pm 45})]_s$	2.428 mm (0.0955”)	0.055”	72%	Testing needs be revisited. Improved measurement method may be required.

5 Manufacturing

The work in this chapter was performed by the student project team: Nick Carlucci, Alex King, Eric Rodan, Caitlyn Pellemeier with leadership and guidance from the author. The rest of this chapter is taken from their research (Carlucci et al.).

5.1 Molding Design

Similar to the approach for FEA modeling, the same philosophy of starting simple was taken for the molding and manufacturing process. Thin plates were chosen as the initial shape for molding rather than the complex part. This would allow the students to determine the best molding technique prior to creating a final part mold. This approach, can also be more cost effective than performing a DOE on multiple complex molds.

5.1.1 Composite Manufactured Plate

The composite plate design is a 6 inch x 6 inch x 0.1 inch thick plate with five ¼ inch holes.

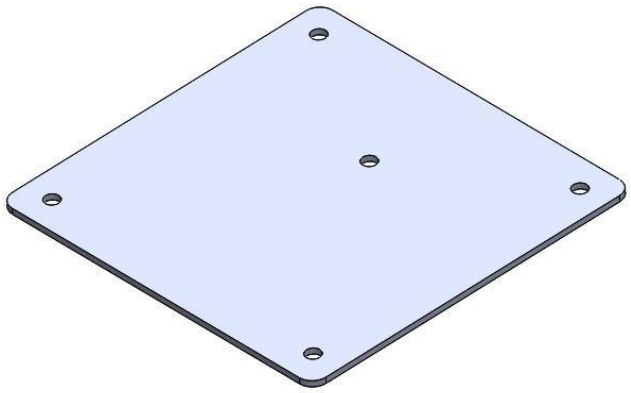

Figure 23 - Composite manufactured plate

The plate was designed to easily fit four machining passes per coupon. The thickness was selected to be the same as the final part. This gave the students experience in composite machining. The four ¼ inch holes in the corners served two purposes. The first is to act as test features for molding. The second function of the holes is to serve as anchor points during machining. The final part has multiple features in it that need to be replicated during molding. This

will enable the team to understand potential difficulties with the final part. The holes will also allow the coupon to be anchored to sacrificial material during machining. The final feature is an offset center hole. This is another test feature for molding. Because the hole is toward the middle of the part, it should have improved resin flow and will provide an example to compare variability of resin flow with the outer holes. The offset was also designed to be a reference point so that the team would be able to easily see which direction resin flowed in final coupons.

5.1.2 Composite Plate Layup

The team created coupons with two different layup patterns. The intent is to test layup patterns that could be used on the final part. One pattern is designed for better machinability and for torsional loading. The second layup is designed to minimize deflection.

The first layup, $[0_2, W_{\pm 45}, \overline{90}]_s$, has zero degree layers on the top and bottom in order to minimize deflection due to bending. The inner 45-degree layers were added to increase torsional strength of the coupon to improve machinability. The 90-degree layer was also added to improve machinability as torsional stiffness is further increased.

The second layup used was $[0_3,90]_s$, which is similar to the first layup with zero degree fibers on the top and bottom for bending stiffness. Instead of the 45-degree weave, the layup adds an additional layer of unidirectional fiber for improved stiffness. At the core, is a 90-degree layer to hold the coupon together. This layup was designed for ease of manufacturing as it only requires unidirectional fiber.

An important consideration when designing the layup was the flow of resin in the mold. Resin tends to flow with the fibers, which as a result can lead to void areas in the part. To reduce the risk of voids, fibers can be oriented in areas to force resin to flow into locations that may be missed. This is crucial for the RTM process because it has a unidirectional resin flow. Similar to a river flowing around a rock, resin flows around features in a mold and can leave voids behind the features. Adding 45 degree and 90 degree laminae to the layup gives the resin a path to follow, forcing resin into problem areas.

5.1.3 Liquid Compression Test Plate Mold Design

The test plate for the LCM molding was designed to produce coupons from the layup above with a simple mold design. The mold is separated into a top and bottom as shown below.

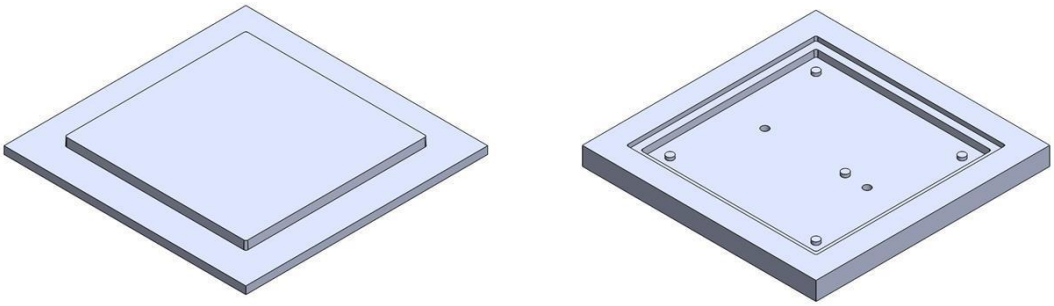

Figure 24 - LCM mold design

The extrusion on the top portion of the mold indexes with the inner cavity of the bottom mold with an overlap of 0.125 inch. The design included a 0.005 inch gap between the top extrusion and the bottom cavity all around the mold to allow excess resin to flow out of the part cavity and into the overflow shelf. The overflow shelf surrounds the mold giving a cubic inch of overflow volume for excess resin or air. There are five ¼ inch extrusions in the bottom portion of the mold to produce the coupon holes. The bottom of the mold has two 0.252 inch holes which will each hold a ¼ inch dowel pin that was used to eject the part after molding process is complete. Additionally, the molds have draft angles of 2 degrees to decrease the difficulty of part removal.

Molds were dimensioned and tolerance so that they could fit into one another with designed 0.005” gap around the edge for resin flow into the overflow shelf. Flatness and parallelism tolerances were added to both the top and bottom of the mold cavity mating surfaces. This controls flatness and parallelism of the actual composite plate.

5.1.4 Resin Transfer Test Plate Mold

The test plate resin transfer mold was designed to incorporate all the features required to successfully perform the RTM process while maintaining geometry that is simple and easy to manufacture. The mold is created in two halves, a top and bottom as shown in Figure 25 - Resin transfer mold design Aluminum was chosen for these molds due to cost and ease of

manufacturability, as well as lead time. The CTE of aluminum compared to carbon fiber epoxy was considered in the design of the molds.

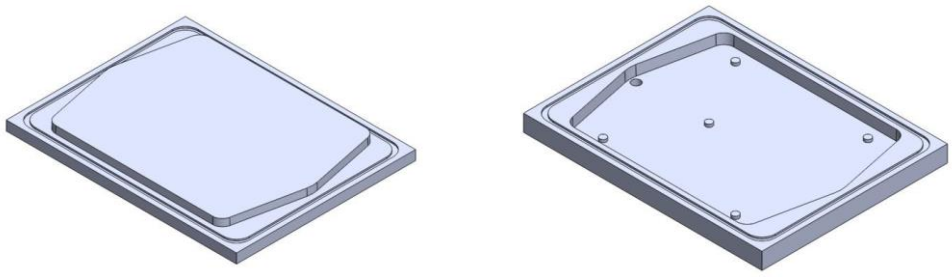

Figure 25 - Resin transfer mold design

The extrusion on the top half of the mold indexes with the cavity on the bottom half of the mold, sliding into one another. The two halves slide together until the outer mating surfaces containing the gasket groove meet one another, leaving a 2.6 mm cavity that will become the part. The indexing walls have 0.025 inch of clearance around the entire perimeter and are cut with a draft angle of 2 degrees for part ejection. There are two ports on the bottom half of the mold, one inlet and one outlet that are tapped with 0.125 inch NTP thread-to-hole barbed fittings. The angled sides on the front and back of the mold cavity act as manifolds for resin to freely flow. This helps the resin flow pattern during the resin transfer process as the resin will be able to spread out to the entire width of the part before it begins to flow through the carbon fiber. The five, ¼" diameter extrusions on the bottom half of the mold will create the five holes of the test plate. As the mold needs to remain completely sealed during resin transfer and curing process, a gasket channel was added around the perimeter of the mating surfaces on both halves of the mold. The gasket channel accepts a 0.125" gasket stock that was cut to length and adhered to one side of the mold. For the RTM mold, holes for ejector pins were not added as they could cause a problem with mold sealing. In place of ejector pins, the intent is that epoxy that cures to barbed fittings will allow the plate to be pushed out. However, the barbed fittings will require release agent so that they can be easily knocked out.

5.1.5 Dry Carbon Fiber Preparation

Since carbon fiber is shipped on continuous rolls, it needs to be cut into the proper shape before it can be placed in the mold for layup. The test plate requires 6” by 6” squares of carbon with 5 accurately placed holes that do not distort the fiber. To achieve this, a template was created out of medium density fiberboard (MDF). The MDF was cut to the shape of the test plate with the 5 holes cut into the shape. The holes in the template are oversized to accommodate a 5/16” diameter punch.

Five holes were cut into the fabric to the oversized diameter of 5/16” for a few reasons. The first is that oversized holes in the fabric will keep the carbon fiber from directly touching the side of the hole which could result in improved surface finish. Allowing some clearance between the hole and the carbon fiber also makes the process of placing the dry fabric in the mold without distorting the fibers easier to achieve.

The entire cutting process was performed on a cutting mat. First, a cutting wheel is run around the perimeter of the template and then the holes were punched out with a sharpened shear punch. The pressure on the template will hold the fibers in place around the holes being punched out, which prevents distortion. To prevent distortion, epoxy-compatible temporary spray adhesive can be used. These types of adhesives are applied to dry fabric and allowed to briefly cure prior to cutting. Once the fabric is cut to the proper shape, and placed in the mold, heat can be applied to evaporate the adhesive.

5.1.6 Mold Release Testing

Mold release was tested to ensure that resin in deep cavities and hole features can be removed easily. Three coats of mold release wax were applied to the entire surface of both top and bottom of molds. The release wax was allowed to dry prior to applying mold release agent over the wax coating. These steps are crucial for RTM mold around the barbed fittings and around the ejector pins for the LCM process. The mold release will help reduce the risk of parts sticking to these components, which could then cause parts to be damaged.

5.1.7 **Molding Safety Considerations**

While performing wet layup molding processes, there are many safety and cleanliness considerations. These considerations include using epoxy compatible containers, protecting workers from carbon splinters, avoiding inhalation of chemical fumes, preventing burns from high temperature molds, and keeping the work area clean.

Using epoxy compatible materials during the layup process is a must. If materials are not epoxy compatible, then the epoxy could react with the container, and potentially melt the container, leaving a slurry of epoxy and plastic. Epoxy compatible materials will include mixing pots, stirring sticks, vacuum and resin lines, catch pots, brushes, and squeegees. All of this material was ordered from composite specific companies.

Cured carbon fiber, especially parts with unfinished edges, can easily splinter or cut the handler. Therefore, protective gloves will be worn while handling unfinished, cured carbon fiber epoxy parts.

Respirators will be worn during the molding layup and cleanup as many chemicals used during layup process can be harmful if inhaled. These chemicals include mold release spray, acetone, and resin epoxy. As an additional precaution, the layup was performed under a ventilated hood. This will help to evacuate fumes from the work environment.

Burn risks are present during the curing cycle as molds are heated to high temperatures. To mitigate this risk, the molds will be left in the press until they have completely cooled. An additional precaution will be taken by wearing leather gloves for handling all molds after they have been through the press process.

Wet composite layups are banned in the composites lab due to safety risks. In order to obtain special approval to perform the layups, a complete safety plan and work instructions for molding were required. The safety plan and method sheet were reviewed by the Professor prior to approval to perform the layups. The safety plan included provisions for preventing spills by creating wood bases with cutouts for mixing cups. This prevents cups being accidentally knocked over from bumping or movement. Additionally, the work area had two layers of protection on work surfaces and on the floor surrounding the work bench. The first level of protection is a thin layer of plastic,

and the second layer is absorbent paper which could slow the flow of epoxy in the case of a spill. The floor was covered with large sheets of cardboard, to aid in absorbing spilled epoxy. These sheets can then be removed and discarded without damaging the floor. The cardboard was taped down to prevent a trip hazard. In order to simulate risks and ensure proper safety measures are in place, a mock manufacturing process was performed, looking for areas to improve safety and mitigate spills.

5.2 Composite Plate Molding

To prepare the fiber for the molding process, it needed to be cut into the shape of the mold. To accomplish this, the team created templates that matched the dimensions of the mold. An example of a template can be seen below in Figure 26.Figure 26 - Layup template and punch

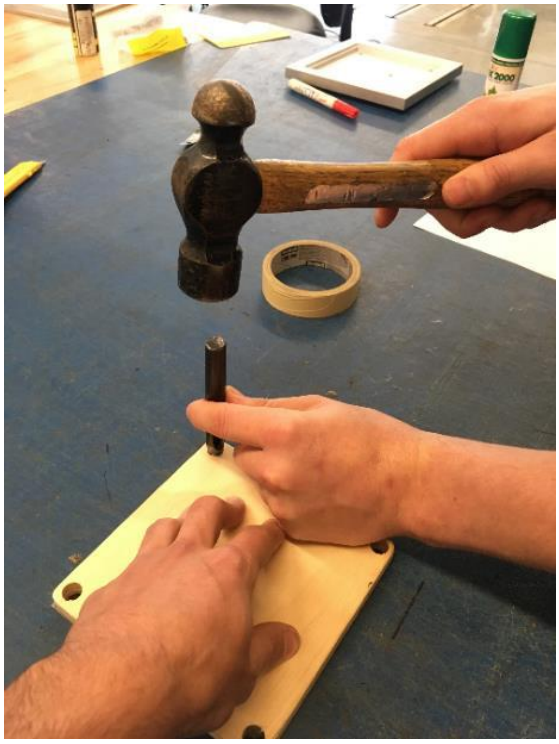

Figure 26 - Layup template and punch

When using the exact sized template, the fabric layers were too big to fit into the mold. This resulted in fabric curing at the edges of the part. After the first molding process was completed with the exact template, the team decided to use a template with undersized dimensions to improve

the molding process. The undersized template had the same dimensions for the hole features, but the length and width were decreased by 1/8". Fabric curing around the edges was eliminated with the undersized template. This became the process for subsequent templates.

For the first molding test, the team attempted to create features using a blade. However, this process was slow, labor intensive, and did not produce the expected results. Additionally, the holes were often not in the correct location, nor were they the correct size. The team decided to switch to a punch for adding circular features. This led to holes that were consistent in size and location. However, tool life needs to be monitored as the shearing of the hard carbon on the punch, led to the punch becoming dull over time. Further study of punch lifetime would need to be a consideration in a production environment.

Figure 27 - Manufactured plate trial with edges curing to mold

5.3 Liquid Compression Plate Molding

Plates were initially planned for manufacture using purely unidirectional fabric. However, the composite would be incredibly brittle in the transverse axes. This would likely lead to a higher risk of damage while removing the plate, as well as during subsequent machining steps. To mitigate this risk, weave layers were added for strength in transverse axis. The first plate trial used

$[0_2, (W_{0/90})_2]_s$. The intent of this layup was to design the plate for maximum stiffness in bending, while providing manufacturability. However, the unidirectional fiber on the top and bottom of the plate made the part brittle when removing the part from the mold. The plate splintered when removed from the mold. After this failure, the layup was further changed to $[W_{0/90}, 0_2, W_{0/90}]_s$. The weave on the top and bottom of the plate reduces bending stiffness, but improved manufacturability.

Figure 28 - Initial manufactured plate trial

5.3.1 LCM Mold Preparation

Preparation of the molds begins with removing any dry epoxy that may be remaining from a previous test. The next step is the application of release wax. The wax is rubbed onto the top and bottom mold, allowed to sit for a few minutes, and then wiped away. This process is repeated three times to ensure the plate will come out of the mold. Next, the mold is placed in the fume hood and

Figure 29 - LCM mold preparation

three layers of non-stick spray is applied, allowing each layer to dry between applications. The molds are now ready for the process.

To prepare the fiber, the wooden template is placed on the fabric and four squares are cut out of both unidirectional fiber, and the weave, using a circular razor cutter. Next, the eight squares are stacked with the template placed on top. Then the punch is used to cut five holes in each of the fabric squares. This ensures that all the holes lineup to create consistent features on the final part. It was found that the unidirectional fiber would come apart easily because there are no fabrics in the transverse direction to hold the part together. To mitigate risk of separation, temporary adhesive spray was added to the fabric prior to being placed in the mold.

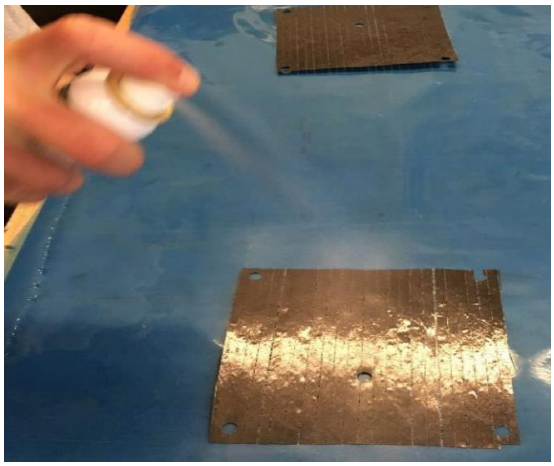

Figure 30 - Fiber cutting and preparation

The resin and the hardener must be measured and mixed before the molding process can begin. A triple beam balance was used to measure out the desired mass of the resin. Next, the proper amount of hardener was calculated for the resin system. A ratio of 1 : 0.277 was used. Then the necessary amount of hardener was measured, added to the resin, and mixed. Syringes were used to fill measuring cups because they provide flexibility to add small or large amounts of material. Care had to be taken to avoid overmixing and creating air bubbles within the resin mix. Once all the materials were prepared, the molding process begins.

First, the bottom of the mold is coated with a layer of resin. This ensures that air will not be trapped in the mold beneath the first layer of fabric. Next, the first layer of fabric is added. After

the fabric is in the mold, another layer of epoxy is poured over the fabric and evenly spread. This is done using brushes and Q-tips. The team was very careful to ensure that the fabric was fully coated in resin to minimize voids within the part. After the resin has been added, another layer of fabric is placed into the mold. The process is repeated for all eight layers of the layup.

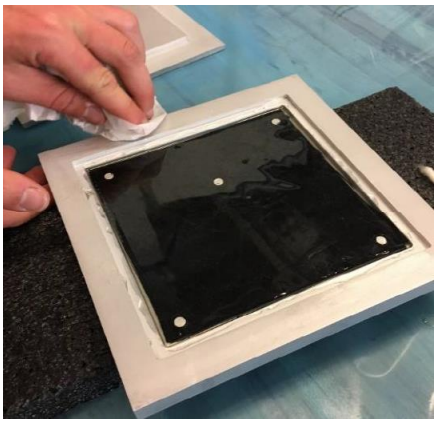

Figure 31 - Layup process example

After adding all layers and resin, the mold is closed and clamped. The heated press in the composites lab was not able to apply the needed pressure, so conventional c-clamps were used to close the mold. Since the press could not be used, heat could not be added to the parts during the molding process. This was unfortunate, but did not limit the experiment. It is recommended to use a heated process in a production environment to maximize stiffness and curing.

Figure 32 - Clamped mold for curing

When closing the mold, one side was slowly lowered and tilted down. This was to allow any air bubbles to escape and prevent voids in the final plate. The plate was then allowed to cure for at least eight hours. After the mold finished curing, ejector pins were used to remove the plate. The mold design had two ¼" ejector pins. To eject the plate, a scraper was used to slide in-between the top and bottom mold pieces to remove the top of the mold. Next, a 3-inch by 6-inch plastic scraper was placed over the ejector pins and tapped with a hammer until the plate rose out of the mold. Sometimes the plate would not get pressed out of the mold and the excess resin had to be chipped from the overflow shelf. This would make it easier for the ejector pins to push the part out of the mold. Overall, the testing found that the ejector pin methodology was slow and created inconsistent results. The design was improved by creating discs for the final mold design. The additional area of the discs combined with threaded screws could improve the ability to remove parts.

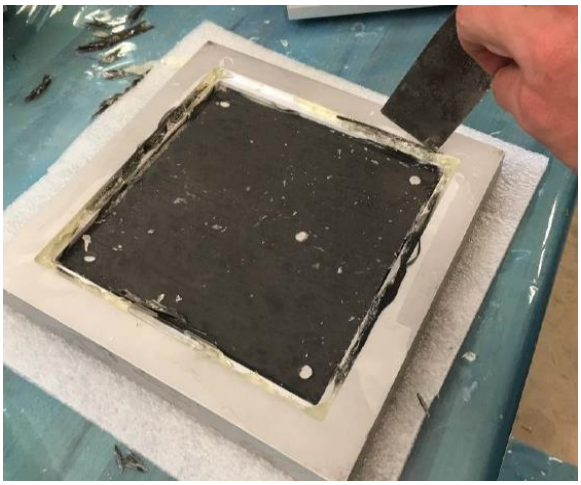

Figure 33 - Removing plate from mold

5.3.2 LCM Plate Molding Results

Six LCM tests were performed following the molding procedure. The results are summarized below.

Test 1:
Shown in , the team used weave for the entire part.
Layup: $[(W_{0/90})_8]T$
Visual Inspection: Three very large air pockets on the top of the coupon, excellent surface on the bottom and matches tolerances well
Voids: Large air pocket on top of coupon and small voids throughout.

Test 2:
First testing using original design layup. Coupon was very brittle because of unidirectional fiber on the outside layers and splintered very badly when removed from the mold.
Layup: $[0_2, (W_{0/90})_2]s$
Visual Inspection: Coupon completely splintered and ruined.
Voids: Cannot determine because of the state of the coupon.

Test 3:
First test using redesigned layup with weave on the outside to prevent cracking when removing from mold.
Layup: $[(W_{0/90}), 0_2, (W_{0/90})]s$
Visual Inspection: Coupon looks very good. Very flat, sharp edges, well defined features, smooth surfaces, easily removed from mold.
Voids: Large air pocket on top of the coupon and small voids throughout.

Test 4:
This test was the same as the previous with addition of a small amount of heat before closing the mold. Shown in Figure 34. This will cause the air bubbles to rise out of the resin and eliminate voids.
Layup: $[(W_{0/90}), 0_2, (W_{0/90})]s$
Visual Inspection: Came out of the mold easily, features and dimensions look good. Almost no leftover epoxy left behind on the mold.
Voids: 2-3 small voids.

Figure 34 - Heating LCM mold to eliminate air bubbles

Test 5:
This test was the same as test 4 except the unidirectional fiber was not sprayed with temporary adhesive. It is believed that the temporary adhesive may be contributing to voids.
Layup: [($W_{0/90}$), 02, ($W_{0/90}$)]s
Visual Inspection: More difficult to remove from the mold than previous tests. Circular markings in fiber around ejection pin locations on coupon.
Voids: 2-3 small voids.

Test 6:
Shown in Figure 35, this test was the same as test 4 except epoxy was degassed for 5 minutes before adding it to the mold to remove air and prevent voids.
Layup: [($W_{0/90}$), 02, ($W_{0/90}$)]s
Visual Inspection: Easily removed from mold, features and dimensions look good.
Voids: 2-3 small voids

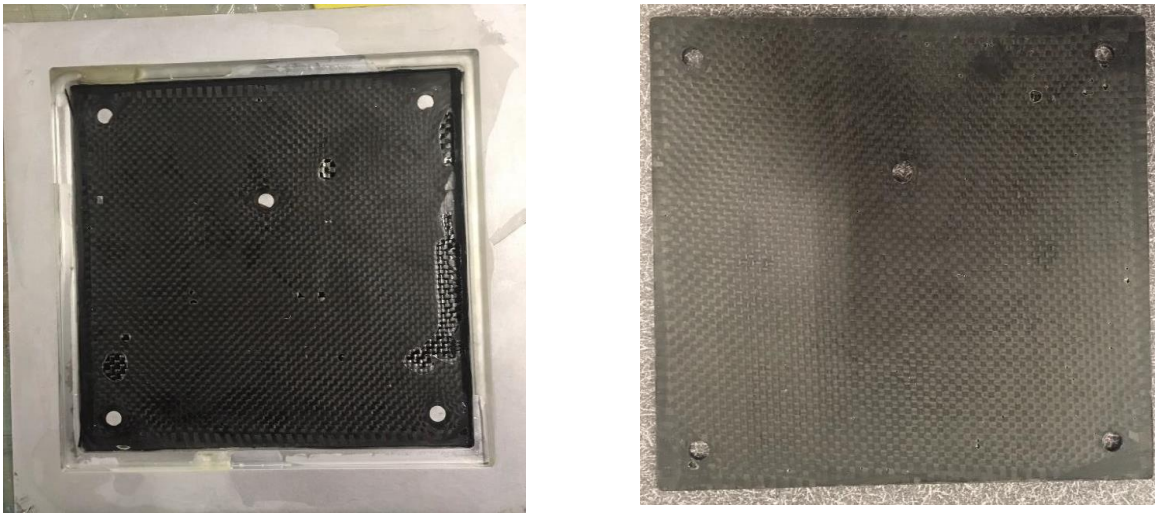

Figure 35 - (L) Test plate 1 with a large air pocket. (R) Test plate 6 with 2-3 small voids

The team found LCM molding to produce better results than the RTM process. The LCM offered a more consistent application of epoxy to the fibers and produced relatively high quality parts that match the mold. The ejector pins need to be larger to improve ease of part removal and reduce stress on the part during removal. It was also determined that an improved method for ejecting parts would be to use threaded holes with bolts to slowly push the part out of the mold. This eliminates the impact of using a hammer on the pins, reducing impact risk on part.

5.4 Resin Transfer Plate Molding

The RTM molding process was performed simultaneously with the second LCM test. As a result, the first RTM layup was $[0_2, (W_{0/90})_2]s$. As previously stated, the it was determined that this layup was difficult to remove from the molds due to unidirectional nature of the fiber. The second RTM test was conducted using the standard $[(W_{0/90}), 02, (W_{0/90})]s$ layup.

Upon inspection of the machined mold, the team found that the holes for the inlet and outlet valves had not been tapped. The taps were added by the team in the Mustang 60 workshop as shown in Figure 36. This serves as a reminder to validate what is being purchased from sub-tier vendors meets the specification.

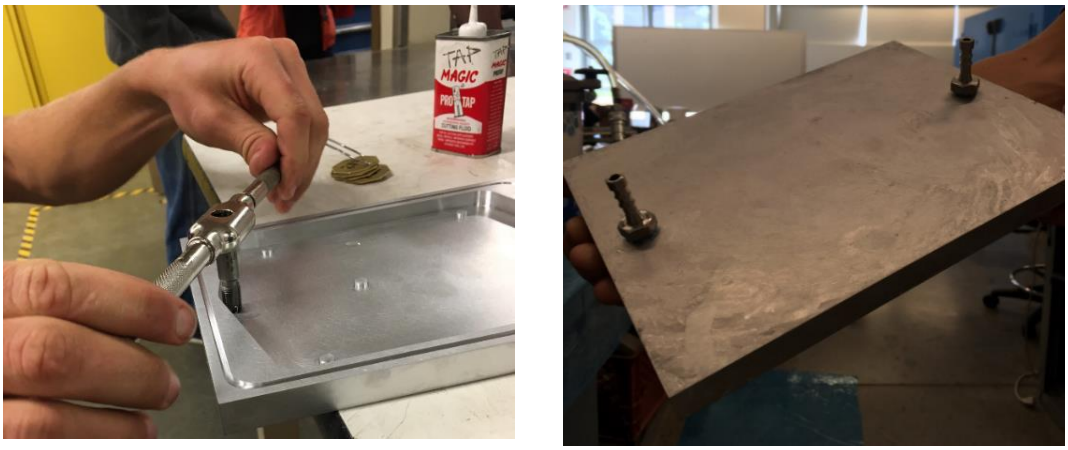

Figure 36 - Tapping holes for inlet and outlet valves

5.4.1 RTM Molding Process

After mold preparation, fiber is stacked in the mold per the desired layup. Next the gasket is added to the groove around the edge of the mold, this ensures the vacuum will not leak. The mold is then clamped. The prepared mold with fiber and gasket is shown on the next page.

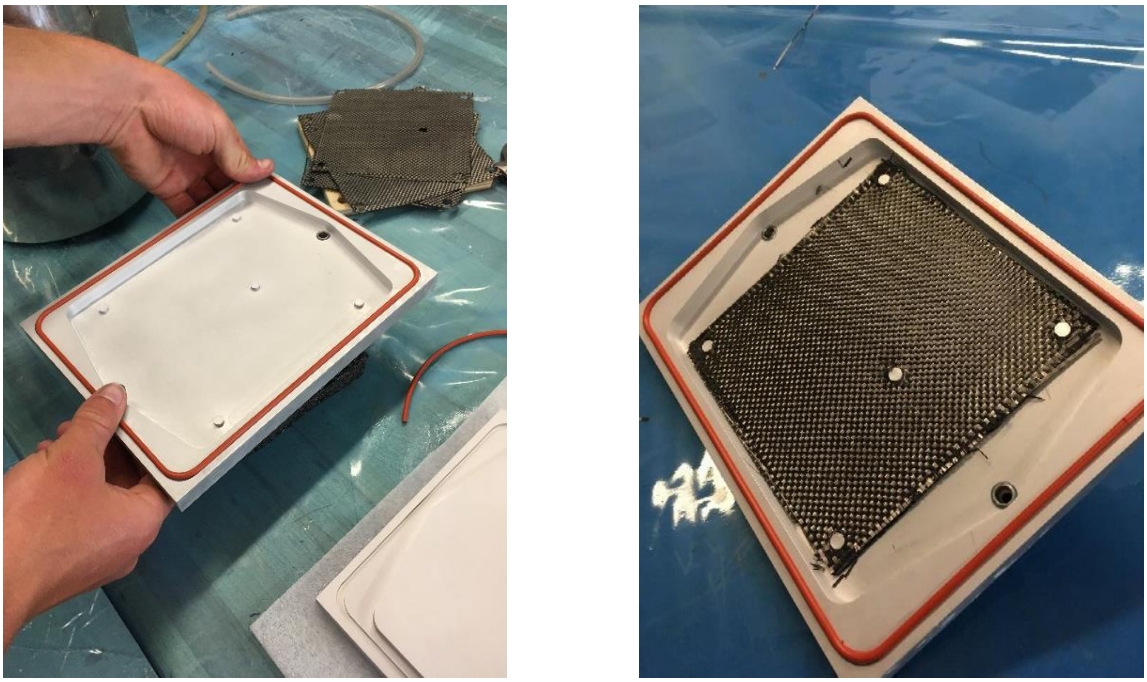

Figure 37 - Adding gasket and fabric to resin transfer mold

Once the fabric is in the mold and sealed, the mold can be attached to the resin transfer system. The resin transfer system has four parts:

1. Pump – generates a vacuum in the tubing
2. Catch Pot – Used between the mold and pump. Contains a small cup to catch resin that has flowed out of the mold
3. Mold – Where the fiber and resin are mixed to create a composite part
4. Epoxy Reservoir (not shown) – Reservoir for epoxy that vacuum pulls into the mold

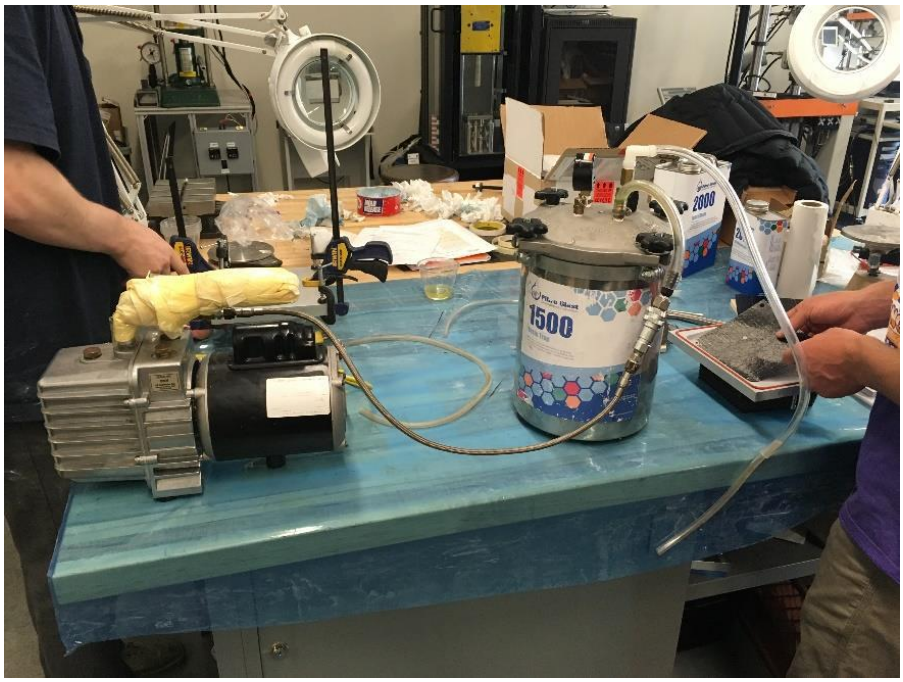

Figure 38 - Resin transfer setup showing pump, catch pot, and mold

After the components have been connected properly, the pump is turned on, vacuum is created, and the resin begins to flow into the mold. The mold is oriented so that the resin flows upward, which encourages the resin to spread evenly throughout the mold. As the mold fills resin begins to leave the outlet valve of the mold. The process is continued until air bubbles can no longer be seen in the tubing at the outlet of the mold. This indicates that resin has completely filled the mold. At this point the inlet and outlet tubes are closed to maintain the vacuum in the mold and the pump is switched off. The plate is then allowed to cure for several hours to ensure the epoxy has fully hardened. After the plate has been allowed to fully cure, the mold is split open and the coupon is removed.

5.4.2 RTM Plate Mold Results

Test 1:
Using original design layup. Pump going full power created a vacuum of 25 hg. Resin was pulled into the mold very quickly and the air bubbles disappeared from the outlet after only two minutes. The team also noted that some fiber was pulled with the resin out of the outlet port into the tubing.
Layup: $[0_2, (W_{0/90})_2]s$
Visual Inspection: Fiber was not full saturated with resin and uniform coupon did not form, see Figure 39.
Voids: Cannot determine because of the state of the composite.

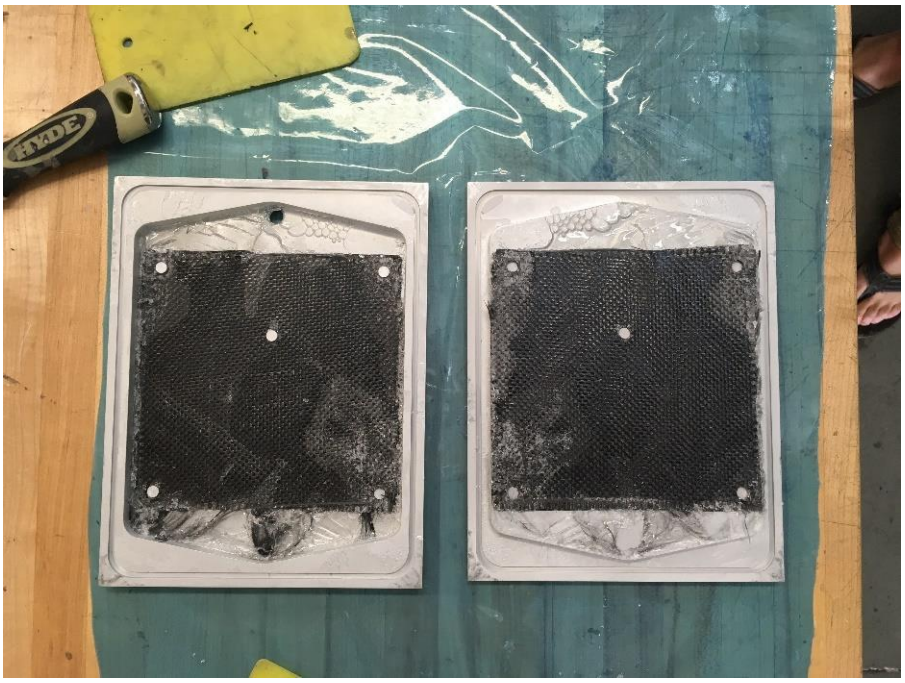

Figure 39 - Results of RTM test 1

Test 2:
After unsuccessful first test the team decided to use a much lower vacuum pressure to pull the epoxy into the mold slower. This should allow for better saturation of the fibers. The team also changed the layup, placing weave on the outside layers to encourage the epoxy to spread side to side. Finally, the team allowed for 5 minutes of additional vacuum time after the air bubbles disappeared from the outlet port, again to ensure proper saturation of the fibers.
Layup: $[(W_{0/90}), 02, (W_{0/90})]s$
Visual Inspection: Fiber was not full saturated with resin and uniform plate did not form, see Figure 40.

Figure 40 - Results of RTM test 2

After the first two resin transfer molding tests completely failed to produce a usable coupon, it was determined that LCM should be the molding process for subsequent coupons and for the final prototype part molding.

5.5 Final Part Mold

Using experiences from designing the part layups with coupon molds, the team was able to incorporate many lessons learned into the final part mold. In the coupon mold, there were a few key problems that occurred, which needed to be addressed in final mold design. The first of these problems was that the ejector pins only pushed on a small surface area of the coupon. This put a high stress concentration on a small area of the coupon while trying to eject the part from the mold. This led to coupons cracking in some cases. The second problem with the ejector pins was that they did not have a way of staying at the proper height, and there was no mechanism to hold them securely in the mold during the molding process. This issue caused small indents in the coupon since the pins could not be held completely flat with the coupon during molding. Additionally, the ejector pins had to be tapped with a hammer to push the coupon out of the mold. This also created high impact forces on the coupon during removal.

To solve the problems with ejector pins, an improved ejector pin design was implemented into the final part mold. The final part uses three 0.75” diameter ejector discs that are inlaid flush

into the mold surface in order to better distribute the load during ejection process. Behind the discs, there are through holes that are tapped with 10-32 threads. Threading the ejector disc holes allowed the team to put machine screws in the holes. This way consistent ejection force could be applied to the part.

Figure 41 - Bottom half of LCM mold for final part

The addition of the ejector discs and threaded ejector pins worked very well in making the process of part ejection more controlled and consistent. Each machine screw pushing on the ejector disc was sequentially turned 180 degrees, which evenly pushed the part out of the mold.

In order to test the molding process to the fullest extent possible, the team chose to mold nearly all features of the final part. This includes small diameter holes, chamfers, and complex slots. There were some more complex features that would be suggested as future research.

The rest of the final part mold was designed using the same concepts that were used in the coupon mold, including a channel around the perimeter of the part for excess air and resin to flow into. The profiles of the top and bottom mating with one another to provide mold alignment and a small clearance gap between the two halves of the mold to allow resin and excess air to flow into the perimeter channel.

5.5.1 **Final Part Layup**

Two prototype parts were created within the timeframe of this research. It was chosen to perform two separate layups for the prototype parts. The layups were $[0_2/(W_{\pm 45})_2]_s$ for prototype 1, and $[W_{\pm 45}/0_2/ W_{\pm 45}]_s$ for prototype 2. The layup for prototype 2 was chosen based on the coupon

layups success in previous trials. However, it was known that this layup does not maximize design for stiffness. Therefore, a stiffer layup was proposed for prototype 1, incorporating learnings from coupon trials to ensure transverse stiffness for molding, handling, and manufacturing.

Similar to the coupon molding process, a template was made to aid in cutting the proper shape for the dry fiber. The template was extremely helpful in creating the outer perimeter of the part. However, the slot features of the part were too small for the cutter to create the feature. Additionally, the small holes in the part were smaller than the ¼" holes in the coupons. This meant that the punch could not be used. It would be recommended to further explore using a properly sized punch for the holes in this part. Instead, the slots were cut using scissors and the holes were created by bending the fibers around the hole extrusions in the mold. Overall, this created a messy layup process that is not production worthy.

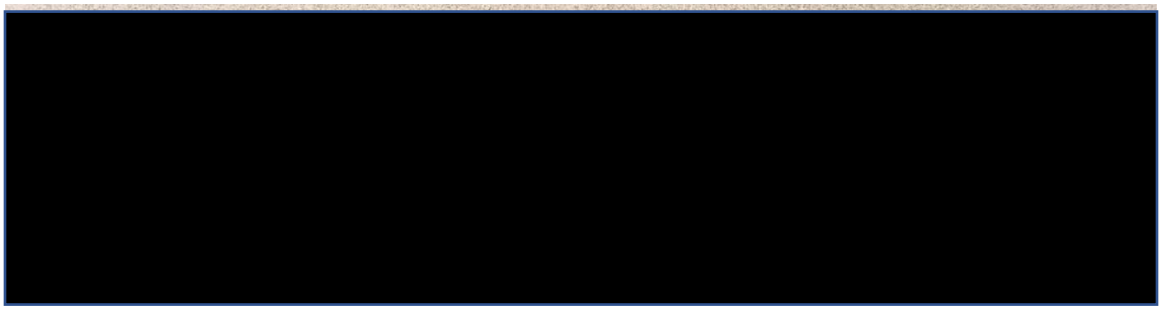

Figure 42 - Layup template for prototype part

5.5.2 **Final Part Prototype Results**

Both prototypes were successfully laid up and ejected from the mold. The ejector disc design proved to be successful as it was able to eject both prototypes without damage. This shows that the coupon mold ejector pins are not optimal, and design improvements to the coupon mold would likely lead to improved plate coupons. Additionally, this means that the fear of using unidirectional

Figure 43 - Prototype part 1

fiber on the out layers of the mold is invalidated, and only required an improved ejector design. However, there is still room for improvement in the final part molding process as both parts contained a few small air pockets.

When the parts were initially removed from the molds they both had a small amount of flashing around the perimeters. This was created from the small clearance between the bottom and top molds being filled with epoxy, as well as the loose fibers that were pulled off the edge of the fabric. This flashing was removed with a razor blade and then the edges were lightly sanded in order to be able to properly fixture the parts for deflection testing. In order to address this problem in the future, an improved cutting method for the fibers is required. Additionally, the tolerances of the production mold could be tightened in order to slow down the flow of air and epoxy while preventing fibers from expanding into the gap.

Figure 44 - Prototype part 2

Another problem that was encountered with the final parts was that some of the through holes were covered on one side with fiber. This is likely due to the fibers moving over extrusion points when closing the mold, which then covered areas that should have been voids. In order to prevent this problem in the future, it is recommended that the extrusions in the bottom half of the mold extend above the surface of the part by a minimum of 0.125". This modification would also require that the top half of the mold be re-cut to allow for extrusions to mate in the top half. Extending the extrusion in the bottom half of the mold would prevent fibers from slipping over the top during mold closure. This technique could also be used for other features as well.

5.6 Final Part Testing

To test the stiffness of the final part, a test method was used to measure tip deflection. To do so, two machinist blocks were used to sandwich the fixed area of the part. To simulate the actual operating conditions, the machines blocks were clamped the same fixed area as modeled in FEA. With the part sandwiched and its tip cantilevered over the table, the part blocks were clamped to the table using a vise grip. Then a magnetic dial indicator was attached to an adjacent

Figure 45 - Deflection test setup

table and pre-loaded slightly by depressing the indicator into the tip of the part being measured. After allowing the tip to be depressed slightly, the indicator was zeroed. Next, two 20g weights were placed at the tip of the part. The deflection was then measured using the dial indicator.

5.6.1 Deflection Testing Results

The experimental deflection testing was performed several times for both the final part layups. An average of the readings was recorded. The final part deflection for prototype 1 was 0.047". The measured deflection for prototype 2 was 0.055". The measured deflections for prototype 1 are in line with models, however the deflection for prototype 2 did not align to FEA model. Further discussion on this topic will be covered in Chapter 6.

5.6.2 Potential Sources for Error

A major source of error came from the dial indicator. The indicator itself requires contact and force to displace the indicator for a reading. Since small deflections are being measured, it is possible that the force required to get a reading on the indicator could have altered deflection readings. It is recommended to move to a non-contact measurement method. Another potential method would be to load more weight than designed to overcome the dial indicator error and remodel the part deflection with larger loading.

6 CONCLUSIONS AND RECOMMENDATIONS

6.1 Summary of Results

The goal of this research was to create a finite element model that can accurately predict stiffness and deflection of an advanced composite part. The second goal was to determine manufacturing methods for prototype parts that could be used in a production environment. To accomplish this, coupons were created and tested using a 3-point bend test. The bend test collected applied force and displacement through a data acquisition system. The test was then modeled in Abaqus® using the same layup and assumed material properties. The results of the Abaqus® model were then modified to fit the force-displacement curve of the experimental results. With material properties from experimental results, a mid-plane shell element model was created to predict prototype part deflection. Two prototypes were created and molded using liquid compression molding. The parts were then deflection tested and compared to the finite element model results. Additionally, a high stiffness part was modeled and compared to similar experimental results performed by a 3rd part. The results are summarized below in the table below.

Table 7 - Modeled deflection compared to experimental results

Part Layup	Model Deflection	Empirical Deflection	% Difference	Comments
M46J model $[0_{10}]$	0.3785mm	Compared to M40J similar part, 0.438mm	13.5%	Aligns to difference between Moduli in M46J and M40J
Prototype 1 $[0_2 / (W_{\pm 45})_2]_s$	1.224 mm (0.048”)	0.049”	2.0%	Well correlated, but limited data
Prototype 2 $[(W_{\pm 45})/0_2 /(W_{\pm 45})]_s$	2.428 mm (0.0955”)	0.055”	72%	Testing needs be revisited. Improved measurement method may be required.

The primary objective was achieved for both the high stiffness (M46J) model and the prototype 1 model. With the test setup it is impressive that the FEA model was within 2% of the experimental results. This is only a data point of 1, but it is promising. Additionally, the M46J model

and results further validate the model appears to be correct. However, the prototype 2 model predicted much larger deflection than experimental results suggest. This is believed to be due to the experimental test setup limitations.

The secondary objective was also achieved. The student project was able to identify methodology and molding design and parameters for a potential manufacturing method. Additionally, they were able to produce multiple plate coupons to be used for 3-point bending tests, which ultimately led to design improvements on the prototype mold. There is still further work that could be done to further improve molding, however the parts met the initial success criteria. Time was not available to validate part dimensions and flatness, so that cannot be evaluated within this research.

6.2 Recommendations for Design Improvement

Based on the modeled and experimental results, it is clear that the driving factor in this system is the bending stiffness matrix, [D]. It is recommended to further research ways to optimize this matrix to increase stiffness and reduce deflection. This would require further study in lamina micromechanics. Ways to accomplish this could through using higher modulus fibers instead of catalog material. However, the higher modulus fiber will drive increased product cost, so a tradeoff table may be necessary to determine the right material. Additionally, similar research could be performed on resin material to improve the stiffness of the lamina. Based on the experimental results, it is estimated that the fiber volume factor was around 30%, meaning that higher modulus resin could improve lamina properties.

Secondarily, the actual part design could be optimized for stiffness. Depending on the customer's design parameters, the part could be optimized to increase the second moment of inertia in order to increase bending stiffness. This could be achieved through different cross sectional shapes, such as "I" beam type stiffeners in the longitudinal direction of the part. Doing so, could optimize part stiffness, but may also make manufacturing more difficult as further complexity would be added to the molding process.

6.3 Proposed Next Steps for Furthering the Project

To further research on this project it is recommended to pursue two paths are proposed. The first path is molding optimization. The recommendations from the students could be implemented to further explore improvements to layup process, and molding process. Research could be performed on optimal settings to improve resin permeation and reduce air bubble risk. Experiments could also be performed on optimal settings to improve composite stiffness. Another recommendation to further molding parameters is to create coupons of a single material type for 3-point bend testing. This will allow material properties to be better analyzed and fed back into the FEA model. Another path may be to look at mold design in more details to validate LCM recommendation over RTM mold types.

The second recommendation is to explore optimal layups for the existing design. With a working model, material properties and layup orientations can be analyzed to improve stiffness. This could be supplemented with code for other software, such as MATLAB® for determining [D] matrix properties. An optimization task could then be created to determine optimal layups and materials. With improved layups, validation testing would be recommended. This could then be furthered with design modifications to part geometry for increased stiffness.

References

Abaqus. *Getting Started with Abaqus*. Dassault Systemes, 2010.

Barbero, Ever J. *Finite Element Analysis of Composite Materials Using Abaqus*. CRC Press LLC, 2013.

Carlucci, Nick, et al. *Manufacturing of a Carbon Fiber Part with Complex Geometry*. 22 Mar. 2018.

Cook, Robert D., et al. *Concepts and Applications of Finite Element Analysis*. 3rd ed., John Wiley & Sons, 1989.

"How Is Carbon Fiber Made?" *ZOLTEK*, 10 Aug. 2017, http://zoltek.com/carbon-fiber/how-is-carbon-fiber-made/.

Kaw, Autar K. *Mechanics of Composite Materials*. CRC Press LLC, 1997.

Mello, Joseph. *Working Papers - ME 412, Composites*. 1 Jan. 2015.

Naik, Rajiv A. *Analysis of Woven and Braided Fabric Reinforced Composites*. National Aeronautics and Space Administration, June 1994. NASA Contractor Report 194930.

Nettles, Alan T. *Basic Mechanics of Laminated Composite Plates*. NASA Marshall Space Flight Center, 1 Oct. 1994. 95N15763, *NASA-RP-1351, M-764, NAS 1.61:1351*, https://ntrs.nasa.gov/search.jsp?R=19950009349.

Park, Soo-Jin, and Gun-Young Heo. *Precursors and Manufacturing of Carbon Fibers*. 1st ed., vol. 210, Springer Netherlands, 2015. *CrossRef*, doi:10.1007/978-94-017-9478-7_2.

What Is Carbon Fiber, Really? | *TORAYCA*® | *TORAY*. http://www.torayca.com/en/aboutus/abo_001.html. Accessed 4 Feb. 2018.

Young, Warren C. *Roark's Formulas for Stress & Strain*. 6th ed., McGraw-Hill, 1989.